LANDBOUWHOGESCHOOL
WAGENINGEN - NEDERLAND

ON THE BOUNDARY LAYER DEVELOPMENT IN ROUNDED BROAD-CRESTED WEIRS WITH A RECTANGULAR CONTROL SECTION

by

M.M. Vierhout

Rapport 3

1973

LABORATORIUM VOOR HYDRAULICA EN AFVOERHYDROLOGIE

LABORATORY OF HYDRAULICS AND CATCHMENT HYDROLOGY
AGRICULTURAL UNIVERSITY - WAGENINGEN - THE NETHERLANDS

ON THE BOUNDARY LAYER DEVELOPMENT IN ROUNDED BROAD-CRESTED WEIRS WITH A RECTANGULAR CONTROL SECTION

by

M.M. Vierhout

1973

REPORT NO. 3

1973

PREFACE

In irrigation, hydrology and water management in general, the accurate measurement of flow rates is a central problem.
Critical flow structures of various types have been designed for this purpose, each having its own special advantages and disadvantages. Broad crested weirs are popular for their sturdiness and for their ability to pass through floating debris and sediment loads during floods. On the other hand friction losses are not insignificant as some length of crest and walls is exposed to the flowing water masses. For practical purposes such losses are accounted for by the introduction of a discharge coefficient into a formula which is derived under the assumptions of a constant energy level and critical flow in a cross section over straight streamlines.
It is a well known fact that this discharge coefficient is not a constant and many empirical studies have been carried out in order to determine its dependance on the changing geometry of the flow pattern.
In order to penetrate into the fundamental aspects of this discharge coefficient it is however essential to realize that the assumption of critical flow and straight streamlines is an approximation and that the essence of friction losses should be studied in the development of boundary layers both laminar and turbulent as a function of the flow pattern and the surface roughness of the measuring structure.
On this basis the present study was initiated in our Laboratory in close cooperation with Mr. Kalkwijk of the Civil Engineering Department of the Delft University. His actual support in the construction of the model and his stimulating comments during the study have been highly appreciated.
As a first attempt Mr. Vierhout's study was limited to the most simple case of a flat horizontal crest with a rounded off upstream nose and parallel vertical side walls.
Not all final answers could be provided for the many questions which arose in this study which required an unusual high accuracy of measurement. Due to a restricted accuracy of the measurement of flow rates some results of this study are more of a qualitative than of a quantitative nature. However, a number of interesting facts have been discovered and helpful techniques have been developed which will stimulate further research.

A principal aspect of boundary layer development is its effect on scaling in the calibration of measuring structures by model studies. It is felt that Mr. Vierhout's work will specially prove its value in the further study of this scaling effect.

D.A. Kraijenhoff van de Leur,
Head of department.

ABSTRACT

In this report a review is given of boundary layer theory and its application to the analytical derivation of a discharge relationship of broad-crested weirs with a rectangular control section. A general method is proposed to derive the boundary layer displacement thickness on the crest from measured velocity profiles, for which two small-scale laboratory models of different sizes have been used. Special attention is paid to the boundary layer development on flat plates in infinite fluids as compared with the development in accelerating flow over the weir. The discharge coefficients derived from an application of critical depth theory allowing for boundary layer growth on the crest are compared with experimental coefficient data, obtained from the laboratory models. No recommendations for the dimensions of the weir in its use as a field structure for flow measurement are made in this report. It was found that a positive pressure gradient at the upstream end of the weir initialy caused the boundary layer to develop faster than in the comparative case of a flat plate in an infinite fluid. The drawdown and consequent negative pressure gradient towards the downstream end of the crest prevent the boundary layer to grow further and even reduce it.

ACKNOWLEDGEMENTS

The writer would like to express his gratitude to Prof.Ir. D.A. Kraijenhoff van de Leur, Staff and Technical Personnel of the Department of Hydraulics and Catchment Hydrology, for their kind and helpful assistance and guidance during his research work.
He also would like to thank Dr.Ir. J.P.Th. Kalkwijk (Head of Laboratory of Fluid Mechanics, T.H. Delft) and Ir. H.N.C. Breusers (Scientific Officer, Hydraulics Research Station, Delft), for their critical and valuable remarks.

TABLE OF CONTENTS

1. INTRODUCTION

During the past few years, séveral attempts have been made at analytically determining the discharge relationship of broadcrested weirs with horizontal crest (virtually straight and parallel flow over the weir), where the flow will change from subcritical into supercritical. The corresponding depth is called the critical depth and it occurs at the critical section. The purpose of these studies is to explain the difference between the actual (viscous-fluid) and the theoretical maximum discharge (frictionless case of non-viscous fluid) by means of the critical depth theory. The ratio of these two discharges is the discharge coefficient which consequently will always be smaller than unity for these structures.

Ippen {1} was the first to introduce the concept of the boundary layer displacement thickness on the crest of the weir. He proposed a discharge equation for broad-crested weirs with rounded off nose and rectangular control section, in which the original specific head is corrected by the displacement thickness. Delleur {2} theoretically investigated the boundary layer development on the crest and compared it with the development of the boundary layer on a flat plate in an infinite fluid at zero incidence. He found the first boundary layer to develop more slowly than the latter one. Hall {3} derived a discharge relationship on the principle of the Ippen equation for a square-edged broad-crested weir. Although one may doubt whether the application of this equation to a case where separation of flow occurs at the square entry edge is permitted, the results agree well with experimental data. Harrison {4} proved the Ippen equation by applying the principle of maximum discharge and analytically derived curves for the boundary displacement thickness on a flat plate in an infinite fluid {5}. He inserted the so obtained relative displacement thickness in the Ippen equation, assuming the critical depth to occur at the downstream end of the crest and the absence of a pressure gradient along the boundary. He compared the theoretical discharges with experimental data of some previous investigators and arrived at satisfactory agreement. Kalkwijk {6} showed that on the basis of different principles and assumptions nearly identical discharge relationships can be derived, however with different expressions for critical depth. The discharge relationships only differ in a coefficient which is a measure for the shape of the velocity profile and consequently for the boundary layer growth. He also gives a general method to determine the discharge of weirs with arbitrary shapes and, for the particular case of a broad-crested weir with

vertical side walls he obtains the Ippen equation. Since no computations of the boundary layer growth on the crest have been made so far, the results for boundary layers in infinite fluids can be used. Kalkwijk {6} and Harrison {14} wonder about the nature of the influence of the negative pressure gradient (acceleration of flow) along the boundary layer on the displacement thickness. They both state that the actual discharge can not be analytically determined, as long as the actual boundary layer development on the crest is not known.

In 1971 Smit {7} started to investigate the flow characteristics of a broad-crested weir model using a weir-table of 40 cm length and a rounded off upstream edge in the laboratory of Hydraulics and Catchment Hydrology at Wageningen. The measurement of velocity profiles and shear distribution with Pitot and Preston tubes respectively, were tested and improved by Smit and Pitlo {8} as the research progressed. Initialy the electronical recording equipment did not produce the required results, but accuracy could be increased by Gaasbeek {9}. On the basis of the experiences of Smit and the research of previous investigators, the laboratory research on boundary layer development was continued by means of a renewed scale model of a broad-crested weir. The structures of stainless steel considered in this report have vertical sidewalls, a broad horizontal crest of either 40 or 120 cm length, preceded by a rounded nose, so that separation of flow is avoided and a nearly parallel flow over the weir occurs. The principle aims of this study were to measure the actual growth of the boundary layer on the crest of the broad-crested weir and to compare the findings with modern boundary layer theory, for which purpose this relatively simple structure offers a good oppertunity. Therefore an attempt is made to develop a general velocity distribution model, from which the boundary layer displacement thickness and velocity distribution coefficients could be easily derived. In addition pressure and shear stress distribution are investigated. Furthermore, a summary is given of the most important analytical derivations of discharge relationships allowing for boundary layer growth on the crest, while the Ippen equation is proved by applying the principle of minimum energy.

The consequences of using either the actual boundary layer on the crest or the corresponding theoretical boundary layer on plates in infinite fluids for the analytical discharge determination are investigated. However, it was not the aim of this study to review the limits of application for flow measurement of this structure, as it was proposed by British Standard 3680 {10}. Furthermore no attempt is made to develop a mathematical model which describes the boundary layer growth on the crest.

It must be emphasized that although this study sheds some light on the complexity

of boundary layer effects in the considered measuring devices, there still remain some important questions, which can only be answered by extensive and accurate experiments in which velocity and pressure distributions are measured simultaneously.

2. ANALYTICAL DERIVATION OF A DISCHARGE RELATIONSHIP FOR BROAD-CRESTED WEIRS

2.1. Non-viscous fluid

Neglecting the energy dissipation (friction losses) in a relatively short and abrupt transition (weir) in open channels as compared to the internal conversion of energy (acceleration), then a unique head-discharge relationship can easily be derived for the modular range of flow.
The specific energy-head H_o above the crest assuming non-curvature of stream-lines (straight and parallel), can be defined as follows:

$$H_o = D + (\alpha)\frac{\bar{u}^2}{2g} = D + (\alpha)\frac{Q^2}{2gA^2} \quad (\alpha \approx 1.00) \qquad (1)$$

in which D = waterdepth, $\bar{u}$ = the average velocity in the considered cross section, g = acceleration of gravity, α = the energy velocity distribution coefficient

$$(= \frac{1}{\bar{u}^3 A}\iint_A u^3 dA),$$

Q = discharge rate and A = wet cross section (see Fig. 1).

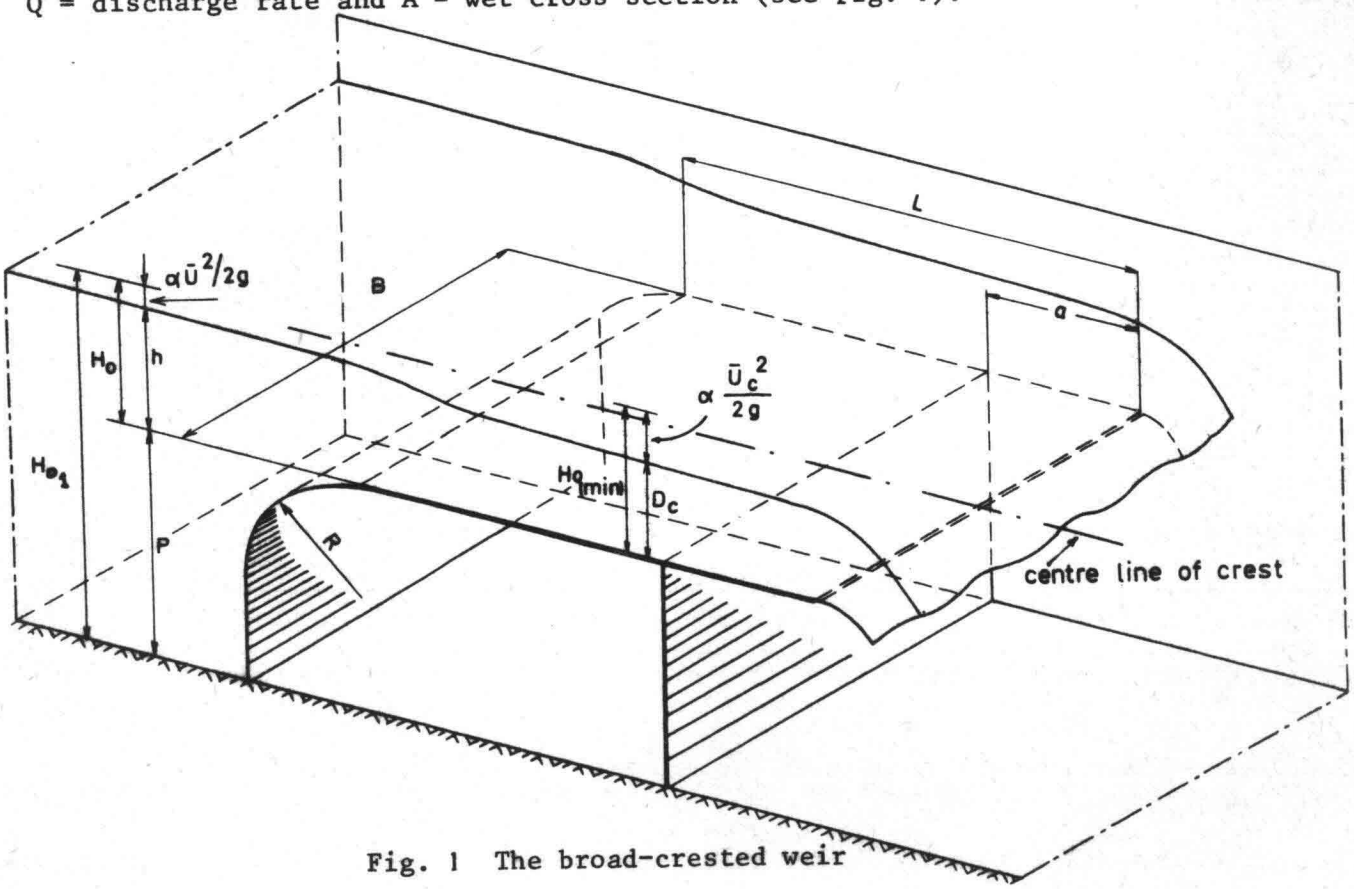

Fig. 1 The broad-crested weir

Applying the principle of minimum energy whereby a constant flowrate Q has to be discharged:

$$\frac{dH_o}{dD} = 1 - \frac{Q^2 B}{gA^3} = 0$$

It follows that for broad-crested weirs with a rectangular control-section (A = B.D. and B = width of the weir):

$$\frac{Q^2}{gB^2 D_c^3} = 1$$

and the critical depth D_c which occurs for the minimum value of H_o is:

$$D_c = \left(\frac{Q^2}{gB^2}\right)^{1/3} \qquad \ldots\ldots\ldots (2)$$

From this it follows that for $H_{o(min)}$ {19}:

$$H_{o(min)} = D_c + \frac{Q^2}{gB^2 D_c^3} \cdot \frac{D_c}{2} = \frac{3}{2} D_c \qquad \ldots\ldots\ldots (2a)$$

which yields for the critical velocity $\bar{u}_c$:

$$\bar{u}_c = g^{\frac{1}{2}} \cdot D_c^{\frac{1}{2}} \qquad \ldots\ldots\ldots (3)$$

or in a more conventional form:

$$Fr = \frac{u_c}{(gD_c)^{\frac{1}{2}}} = 1 \qquad \ldots\ldots\ldots (3a)$$

(the Froude number Fr equals unity for critical conditions). As stated before, the assumption is made that the energy head of the critical section equals the original energy head in the approach channel H_{o_1} and thus:

$$H_{o_1} = H_{o(min)} + P$$

in which P = crest height (see fig. 1). (From here on the original specific head is denoted by H_o, omitting the subscript (min).)
If the crest section becomes critical, it is possible to determine the relationship between the theoretical discharge rate Q^{th} and the specific energy head H_o:

$$Q^{th} = B \cdot D_c \cdot u_c = B \cdot D_c^{3/2} \cdot g^{\frac{1}{2}} \qquad \ldots\ldots\ldots (4)$$

or in a more commonly used form for the rectangular broad-crested weir:

$$Q^{th} = B \cdot \left(\frac{2}{3}\right)^{3/2} \cdot g^{\frac{1}{2}} \cdot H_o^{3/2} \qquad \ldots\ldots\ldots (4a)$$

2.2. Viscous fluid

2.2.1. Correction coefficients

On account of practical purposes one shoud adjust the theoretical discharge relationship (4a) to the effects of viscosity and flow curvature. In order to make this discharge relationship (4a) more operational for discharge measurements in open water courses or channels, it is often written as follows:

$$Q = C_D \cdot C_v \cdot B \cdot \left(\frac{2}{3}\right)^{3/2} \cdot g^{\frac{1}{2}} \cdot h^{3/2} \qquad \ldots\ldots\ldots (5)$$

in which $C_v = (H_o/h)^{3/2}$, h = measured head upstream the crest and C_D = discharge coefficient to adjust for the effects of friction forces of the viscous fluid and curvature of streamlines overhead the crest. The value of C_D was found to be almost constant (= 0.96) for the following limitations {10}:

$$0.008 < H_o/L < 0.33$$

$$0.18 < \frac{h}{h + p} < 0.36$$

in which L = crest-length (fig. 1).

2.2.2. Boundary layer development on the crest

In the ideal case of a non-viscous fluid as mentioned in 2.1. it is assumed that an undisturbed potential flow will occur above the crest. This means that for rectilinear and parallel streamlines the velocity in a cross section perpendicular to the crest will be constant. Near the boundary however a layer of fluid is decelerated because of the resistance to flow caused by the shear at the wall. This relatively thin layer, in which the velocity deviates from the constant ambient velocity, is called boundary layer and can develop in either laminar or turbulent flow. The growth of boundary layers can be theoretically analysed on the basis of a hypothetical flow system {21}.

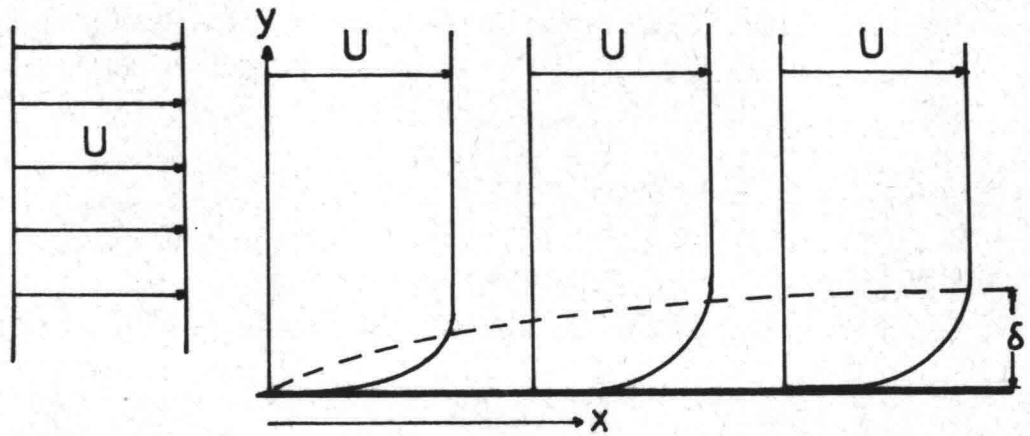

Fig. 2. Boundary layer development on a flat plate in an infinite fluid

If a flat plate is placed (Fig. 2) parallel to the streamlines in an infite fluid with a constant ambient velocity u in the main stream, a velocity gradient $\frac{\partial u}{\partial y}$ will develop near the flat plate. This gradient depends on the roughness of the plate (shear stress) and the degree of turbulence in the mainstream. The velocity very close to the wall becomes zero and the consequential tangential shear stress causes perturbations and instability of flow, which will expand in the downstream direction (Fig. 2). The outer edge of the thus formed boundary layer can be defined arbitrarily as the location where the local velocity equals 99% of constant velocity u in the main stream. The numerical value of the boundary layer thickness δ, in practice will be very difficult to determine, because the distance to the point where the influence of the boundary is negligible can never be measured exactly. (The velocity in the boundary layer approaches the constant velocity u asymptotically!). It is further assumed, that outside the boundary layer the flow is irrotational ($\partial u_x/\partial y = \partial u_y/\partial x$) and therefore potential, for which the energy equation of Bernoulli applies:

$$\frac{u^2}{2g} + y + \frac{p}{\rho g} = \text{constant}$$

(p = local pressure and ρ = density of fluid).

In order to be able to quantify the characteristics of the boundary layer in a more convenient way than by its thickness δ alone, the concept of *boundary layer displacement thickness* (δ_d) is introduced. The displacement thickness is defined

as the distance over which the wall has to be theoretically displaced in order to discharge the same amount of fluid as in the case of undisturbed potential flow. From Fig. 3 it follows how δ_d can be expressed in terms of velocity distribution and boundary layer thickness.

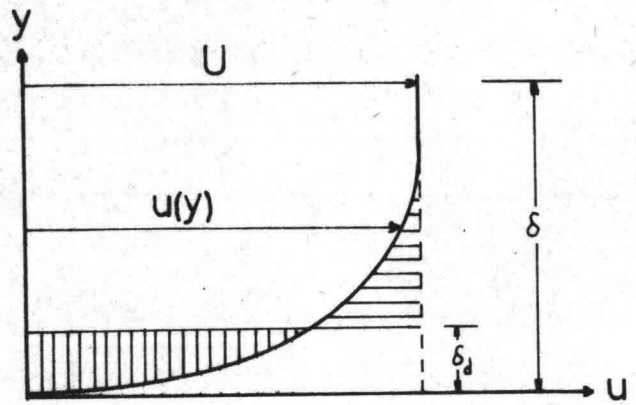

Fig. 3 Boundary layer displacement thickness

In order to meet the requirement of continuity according to the above mentioned definition, one can write if U is the velocity for $y = \delta$:

$$\int_0^D u(y)dy = U(D-\delta_d) \qquad \text{..... (6a)}$$

or, since U is constant outside the boundary layer:

$$\int_0^\delta u(y)dy = U(\delta - \delta_d) \qquad \text{..... (6b)}$$

from which one can deduce δ_d:

$$\delta_d = \int_0^\delta (1 - \frac{u}{U})dy \qquad \text{..... (6c)}$$

It is obvious that the boundary layer displacement thickness can be determined more accurately than the boundary layer thickness, since a small change of δ only causes a negligible change of δ_d. Evidently δ_d is a useful measure to quantify the shape of the velocity distribution in the boundary layer and its thickness. Flow problems in which the boundary layer effects may have great influence (viscous-effects not negligible!), such as weir-or spillway flow, can be analysed theoretically by considering the total flow pattern as potential (irrotational), while at the same time supposing the boundary (crest) to be displaced over a distance δ_d {21}.

A second characteristic of a boundary layer is the *momentum thickness* δ_m. According to the definition of momentum, a small fluid element with a mass of (ρudy) possesses the momentum over a differential time Δt of:

$$(\rho udy) \cdot u \cdot \Delta t$$

The same fluid element has in case of absence of a boundary layer (non-viscous) a momentum equal to (ρudy) . U . Δt. The change in momentum as a result of the friction force at the boundary is therefore:

$$\int_o^{\delta} \rho u(U - u)dy \qquad \ldots\ldots\ldots (7)$$

and because of the continuity principle:

$$\int_o^{\delta} \rho u(U - u)dy = \rho U^2 \delta_m. \quad \text{or} \quad \delta_m = \int_o^{\delta} \frac{u}{U}(1 - \frac{u}{U})dy \qquad \ldots\ldots\ldots (7a)$$

A third characteristic often used in the boundary layer theory, is the *energy thickness* δ_e:

$$\int_o^{\delta} \frac{u}{U}(1 - \frac{u^2}{U^2})dy \qquad \ldots\ldots\ldots (8)$$

Regarding the change in momentum flux along the boundary (7) and bearing in mind Newton's second law of motion, the following expression can be derived {21}:

$$\tau_o = \mu \left.\frac{du}{dy}\right|_{y = o} = \rho \frac{d}{dx} \int_o^{\delta} u(U - u)dy \qquad \ldots\ldots\ldots (9)$$

in which τ_o = shear stress (or tractive force) at the boundary and μ = dynamic vicosity.

In order to derive the shape and thickness of the boundary layer from equation (9), a numerical integration of measured velocity profiles is required. Schlichting {11} obtained from experiments with a flat plate in an "infinite" fluid the following expression for a laminar boundary layer ($R_x = \frac{Ux}{\nu} < 3.10^5$, ν = kinematic viscosity):

$$\frac{\delta}{x} = \frac{5.2}{R_x^{\frac{1}{2}}} \quad \text{or} \quad \frac{\delta_d}{x} = \frac{1.73}{R_x^{\frac{1}{2}}} \qquad \ldots\ldots\ldots (10)$$

in which x = the distance from the upstream edge of the plate.
The local dimensionless friction factor c_f (or drag coefficient) then becomes:

$$c_f = \frac{\tau_o}{\rho U^2/2} = \frac{0.66}{R_x^{\frac{1}{2}}} \quad \ldots\ldots\ldots (11)$$

and the corresponding total friction factor C_f over a length x is:

$$C_f = \frac{F/B.x}{\rho U^2/2} = \frac{1.328}{R_x^{\frac{1}{2}}} \quad \ldots\ldots\ldots (12)$$

in which $F = \int_o^x \overline{\tau}_o \, Bdx$ (total mean shear force) and B = width of plate.

For the turbulent boundary layer ($R_x > 10^6$) over a hydraulic smooth boundary, Prandtl and Blasius were able to derive the thickness δ on the basis of the one-seventh power law of velocity distribution:

$$\frac{\delta}{x} = \frac{0.377}{R_x^{1/5}} \quad \text{and} \quad C_f = \frac{0.074}{R_x^{1/5}} \quad \ldots\ldots\ldots (13)$$

Schlichting {11} also stated that:

$$C_f = \frac{2\,\delta_m}{x} \quad \ldots\ldots\ldots (14)$$

Granville {12} and Schlichting {11} gave the following implicit equation of the total friction factor, for rough as well as smooth boundaries:

$$\frac{0.544}{C_f^{\frac{1}{2}}} - 5.61\, C_f^{\frac{1}{2}} + 0.638 = -\ln\left(\frac{1}{R_x C_f} + \frac{1}{4.84\,\frac{x}{k}\,C_f^{\frac{1}{2}}}\right) \quad \ldots\ldots\ldots (15)$$

in which k = the equivalent roughness height of Nikuradse.
Granville shows further that, if $H = \frac{\delta_d}{\delta_m}$, then follows:

$$\frac{H}{H-1} = \frac{1}{6.64\,\frac{u_*}{u}} \quad \ldots\ldots\ldots (16)$$

in which H = a shape factor of the boundary layer and $u_* = \left(\frac{\tau_o}{\rho}\right)^{\frac{1}{2}}$ is the shear velocity.

Harrison {5} shows how the relative boundary layer displacement thickness δ_d/x on a flat plate, without a velocity gradient outside the boundary layer (ambient

velocity remains constant), depends on the total friction factor C_f.
From equation (14) and (16) it follows that:

$$\frac{\delta_d}{x} = - \frac{C_f}{2\{1 - (6.64 \frac{u_*}{u})\}} \qquad \ldots\ldots\ldots (17)$$

Together with equation (15) the relative displacement thickness of turbulent boundary layers can be calculated for hydraulic smooth as well as hydraulic rough boundaries.
For the transition from laminar into turbulent boundary flow, $3.10^5 < R_x < 10^6$, Dhawan and Narasimha {13} give the following relation:

$$\frac{\delta_d}{x} = (1 - \gamma) \frac{\delta_d^{\,L}}{x} = \gamma \frac{(x - x_t)}{x} \cdot \frac{\delta_d^{\,T}}{(x - x_t)} \qquad \ldots\ldots\ldots (18)$$

$$\gamma = 1 - e^{- 0.412 \{(R_x - R_t)/5 R_t^{0.8}\}^2} \qquad \ldots\ldots\ldots (18a)$$

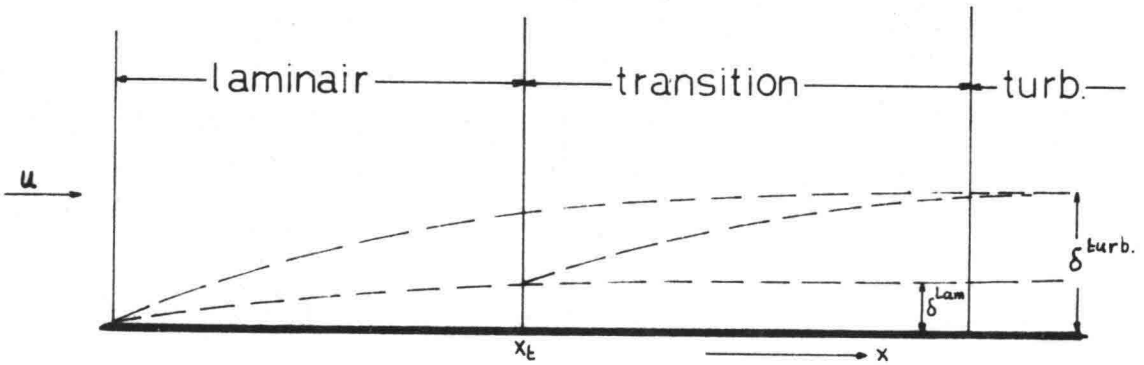

Fig. 4 Transition boundary layer

in which $\delta_d^{\,L}$ = the laminar boundary layer displacement thickness at a distance x from the upstream edge of the plate.
$\delta_d^{\,T}$ = the turbulent dito.
x_t = the place of transition
R_t = $(U \cdot x_t)/\nu$
γ = weight factor

Harrison {5} established useful curves for the relative boundary layer displacement thickness as a function of R and x/k (relative roughness) on the basis of equation (15), (17) and (18). The transition curves were calculated

for the utmost limits of R_t(3.10^5 and 10^6). These curves were slightly modified by Ackers {14} (see Fig. 5.).

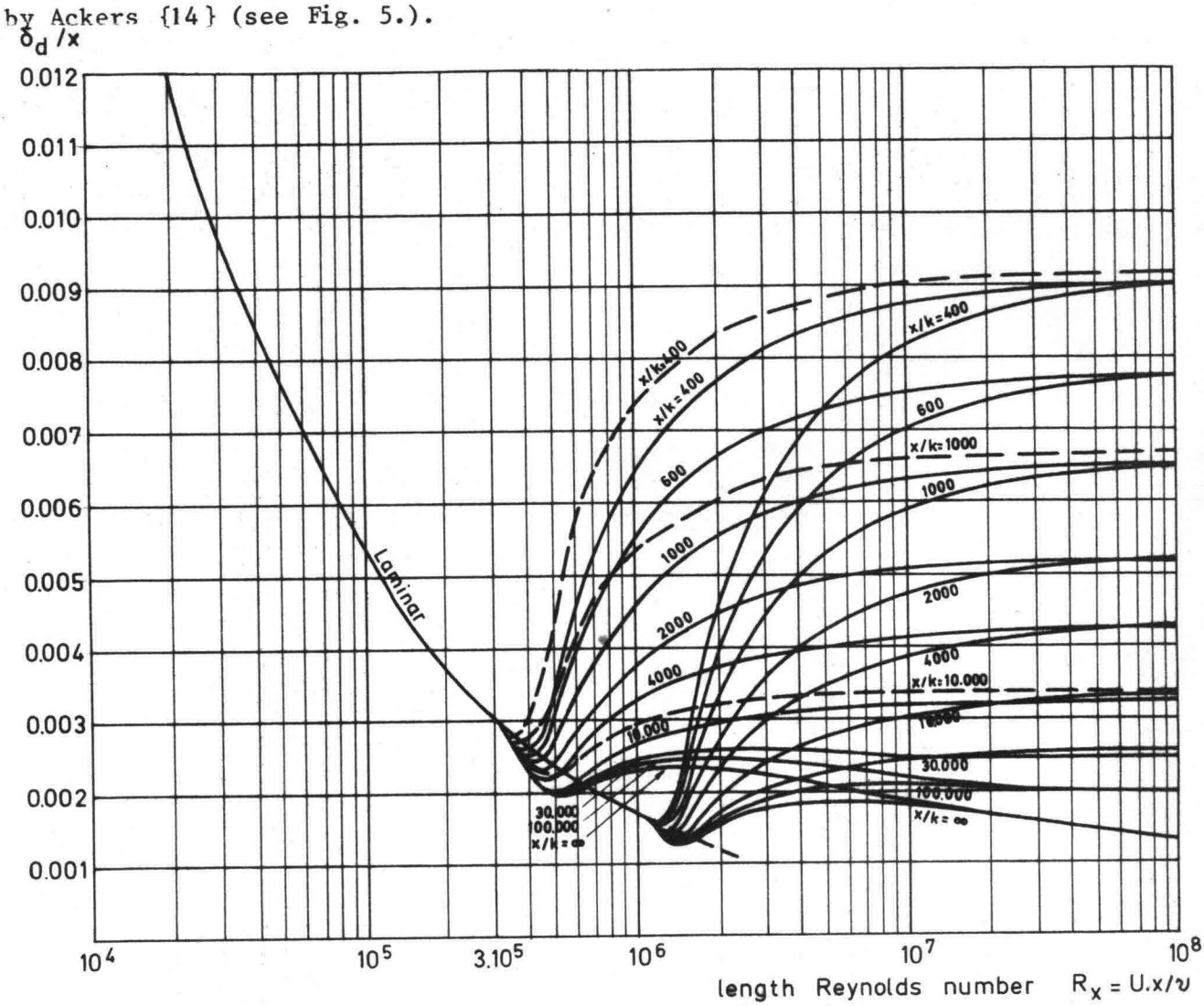

FIG. 5 Relative boundary layer displacement thickness: laminar transition curves for $R_t = 3.10^5$ and $R_t = 10^6$ (A.J.M. Harrison 1967)
— — — Correction published by Ackers

Along the crest of a broad-crested weir, the boundary layer will develop in a rather similar way, however with two major differences:

- negative pressure gradient in the flow direction and therefore an acceleration in that direction ($\frac{dD}{dx} < 0$);
- no rectilinear and parallel streamlines at the upstream and downstream parts of the crest and consequent deviations from hydrostatic pressure distribution.

The question arises to what extent the effects of pressure gradient and flow curvature do affect the boundary layer development on the crest, in comparison to the hypothetical boundary layer development on a flat plate in an infinite fluid. According to Delleur {2} one should expect a boundary layer on the crest to be less developed than the one on a flat plate (see section 3.3.1.).

2.2.3. Discharge relationship

Ippen was the first one to take into account the boundary layer development on the crest while considering the discharge relationship of broad-crested weirs with a rounded-off nose. Although he did not give a derivation of the resulting relationship (in which the original specific head and the width of the weir were merely corrected for the boundary layer displacement thickness δ_d), one can easily show in different ways, that the Ippen-equation may be considered a good approximation.

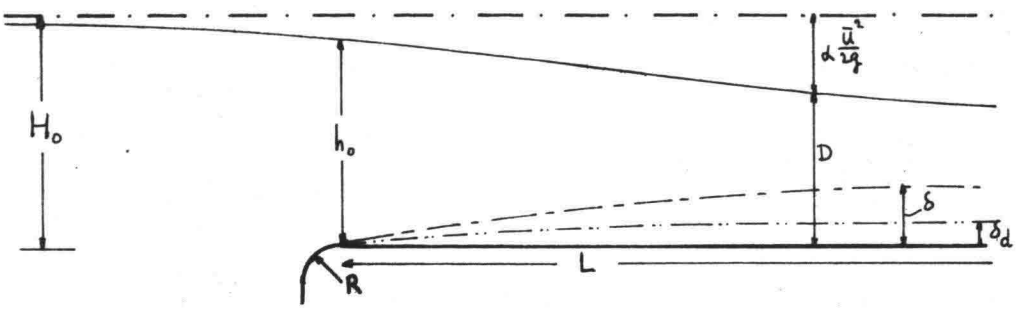

Fig. 6 Definition sketch

Assuming, for example, potential flow outside the boundary layer on the weir, the velocity U outside the boundary layer then is:

$$U = \{2g(H_o - D)\}^{\frac{1}{2}} \qquad \ldots\ldots\ldots (19)$$

Because of the continuity principle and supposing the crest displaced over a distance δ_d:

$$Q = (A - W\delta_d) \cdot U \qquad \ldots\ldots\ldots (20)$$

in which W = wet perimeter and δ_d = the average displacement thickness, which is defined as follows:

$$\delta_d = \frac{1}{W} \iint_A (1 - \frac{u}{U}) dA$$

Equating (19) and (20) it follows for the specific energy head H_o on the crest and by approximation in the approach channel as well:

$$H_o = D + \frac{Q^2}{2g(A - W\delta_d)^2} \qquad \ldots\ldots\ldots (21)$$

With the assumption that the crest section becomes critical at a certain point and by the application of the principle of minimum energy, equation (21) yields:

$$\frac{dH_o}{dD} = 1 + \frac{Q^2}{2g} \frac{d}{dD} \{B \cdot D - (B + 2D)\, \delta_d\}^{-2} = 0$$

or

$$\frac{Q^2(B - 2\delta_d)}{g(A_c - W_c\, \delta_d)^3} = 1 \qquad \ldots\ldots\ldots (22)$$

in which B = the width of the rectangular weir and the suffix c denotes the critical state of flow. Substituting (22) into (21) yields:

$$H_o = D_c + \frac{(A_c - W_c\, \delta_d)}{2(B - 2\delta_d)} \qquad \ldots\ldots\ldots (23)$$

the same result as found by Ackers {14}.
Transforming (23) we find:

$$2(H_o - D_c)\,(B - 2\delta_d) = B \cdot D_c - (B + 2D_c)\delta_d \qquad \ldots\ldots\ldots (23a)$$

or

$$D_c = \frac{2}{3} H_o + \frac{B \cdot \delta_d}{3(B - 2\delta_d)} \qquad \ldots\ldots\ldots (24)$$

Because $B \gg \delta_d$ one may rewrite (24) as an approximation:

$$D_c = \frac{2}{3} H_o + \frac{1}{3} \delta_d > \frac{2}{3} H_o \qquad \ldots\ldots\ldots (24a)$$

which is equal to the result of Harrison {4}, who, however, applied the principle of maximum discharge for a given depth.
From (20) it follows:

$$Q = \{B \cdot D_c - (B + 2D_c)\delta_d\} \cdot \{2g(H_o - D_c)\}^{\frac{1}{2}} \qquad \ldots\ldots\ldots (25)$$

and transforming (24a):

$$H_o - D_c = \frac{1}{3}(H_o - \delta_d) \qquad \ldots\ldots\ldots (25a)$$

Finally, by eliminating D_c from (25), (25a) and (23a) we obtain the following expression:

$$Q = g^{\frac{1}{2}} \cdot (\frac{2}{3})^{3/2} \cdot (H_o - \delta_d)^{3/2} \cdot (B - 2\delta_d) \qquad \ldots\ldots\ldots (26)$$

which is the so called Ippen-equation {1}. In deriving equation (26) it was assumed that δ_d does not depend on the water depth D, which is only justified for turbulent boundary layers along hydraulic rough walls, since in that case δ_d does not depend on the velocity U (and hence the depth) outside the boundary layer {5}.

Kalkwijk {6} shows us, that different basic assumptions lead to nearly the same discharge relationships for critical depth measuring devices with arbitrary shape, however with different expressions for critical depth. Starting with the continuity and momentum equation of a long wave and assuming that the mean velocity in the control section is equal to the propagation velocity of a long wave:

$$\frac{\partial(\bar{u}A)}{\partial x} + \frac{\partial A}{\partial t} = 0 \qquad \ldots\ldots\ldots (27)$$

$$\frac{\partial(\bar{u}A)}{\partial t} + \frac{\partial(\beta\bar{u}^2 A)}{\partial x} + gA\frac{\partial D}{\partial x} = \frac{W\bar{\tau}_o}{\rho} \qquad \ldots\ldots\ldots (28)$$

in which $\bar{u}$ = the mean velocity in a cross-section, $\bar{\tau}_o$ = the average shear-stress at the boundary and β = the momentum-flux coefficient, which is defined as follows:

$$\iint_A u^2 dA = \beta\bar{u}^2 A$$

the direction of the characteristics belonging to the set of partial differential equations (27) and (28) can be found by the determinant method, in which dA = B.dA and β is considered constant with x (is positive in the flow direction), since $\frac{\partial\beta}{\partial x}$ is not known:

$$\frac{dx}{dt} = \beta\bar{u} \pm \{(\beta^2 - \beta)\bar{u}^2 + \frac{gA}{B}\}^{\frac{1}{2}}$$

(B = the top width in an arbitrary prismatic cross section). Disturbances downstream of the critical section can not move in the upstream direction if $\frac{dx}{dt}$ equals zero and therefore:

$$Q = A_c \cdot u_c = A_c \left(\frac{gA_c}{\beta B_c}\right)^{\frac{1}{2}} \qquad \ldots\ldots\ldots (29)$$

If one considers critical weir flow as a gradually varied flow, equation (28) for steady flow becomes:

$$\frac{d}{dx} \iint_A u^2 dA + gA \frac{dD}{dx} = - \frac{W\bar{\tau}_o}{\rho} \qquad \ldots\ldots\ldots (30)$$

After transformation of (30) and introduction of the momentum thickness δ_m, one obtains the backwater curve {6}:

$$\frac{dD}{dx} = - \frac{\frac{W\bar{\tau}_o}{\rho} + \frac{WQ^2}{A^2} \frac{d}{dx}(\delta_d - \delta_m)}{gA - \frac{BQ^2}{A^2}\{1 + \frac{2W(\delta_d - \delta_m)}{A}\}} \qquad \ldots\ldots\ldots (31)$$

Application of the principle, that critical flow occurs where $\frac{dD}{dx}$ becomes infinite (vertical flow profile), results into the following discharge relationship:

$$Q = A_c \left[\frac{gA_c}{B_c\{1 + \frac{2W}{A}(\delta_d - \delta_m)\}}\right]^{\frac{1}{2}} \qquad \ldots\ldots\ldots (32)$$

From the more common equation for steady gradually varied flow (normal backwater curve), one can derive the same equation as (29):

$$\frac{dD}{dx} = \frac{S_o - \frac{W\bar{\tau}_o}{\rho gA} - \frac{u^2}{2g}\frac{d\beta}{dx}}{1 - \beta \frac{BQ^2}{gA^3}} \qquad \ldots\ldots\ldots (33)$$

(S_o = bottom slope)

If $\frac{dD}{dx}$ tends to infinity, equation (33) yields:

$$Q = A_c \cdot u_c = A_c \left(\frac{gA_c}{\beta B_c}\right)^{\frac{1}{2}} \qquad \ldots\ldots\ldots (34)$$

Application of the minimum energy principle yields the wellknown result. The specific energy head is:

$$H_o = D + \alpha \frac{Q^2}{2gA^2}$$

setting $\frac{dH_o}{dD} = 0$, one gets:

$$Q = A_c \left(\frac{gA_c}{\alpha B_c}\right)^{\frac{1}{2}} \qquad \ldots\ldots\ldots (35)$$

Harrison {14} has shown, that α can be expressed in terms of energy thickness δ_e and displacement thickness δ_d:

$$\alpha = \frac{\left(1 - \frac{\delta d}{D} - \frac{2\delta_d}{B} - \frac{\delta e}{D} - \frac{2\delta_e}{B}\right)}{\left(1 - \frac{\delta d}{B} - \frac{2\delta_d}{B}\right)^3} \qquad \ldots\ldots\ldots (36)$$

which is logical, since α depends on the shape and thickness of the boundary layer.

Yen and Wenzel {15} obtained the following backwater equation by application of the energy equations for steady gradually varied flow:

$$\frac{dD}{dx} = \frac{S_o - S_e - \frac{u^2}{2g}\frac{d\alpha}{dx}}{1 - \alpha \frac{BQ^2}{gA^3}} \qquad \ldots\ldots\ldots (37)$$

(S_e = energy slope)
from which we can derive a similar discharge relationship to (35).

It is not possible to prove theoretically, which of the above mentioned derivation procedures is the most justified. Therefore Kalkwijk {6} introduced a general approximative discharge relationship for critical-depth - measuring weirs with arbitrary shape:

$$Q = A_c \left\{\frac{gA_c}{(1 + \varepsilon)B_c}\right\}^{\frac{1}{2}} \qquad (0 < \varepsilon \ll 1) \qquad \ldots\ldots\ldots (38)$$

which represents in fact a relationship between critical depth D_c and Q.
If D_1 is the approximate critical depth that results from:

$$Q = A_1 \left(\frac{gA_1}{B_1}\right)^{\frac{1}{2}} \qquad \ldots\ldots\ldots (39)$$

then it follows from (39) and (21), after ignoring second order terms (compare also with equation (23)):

$$H_o - \frac{W_1}{B_1}\delta_d = D_1 + \tfrac{1}{2}\frac{A_1}{B_1} \qquad \ldots\ldots\ldots (40)$$

This expression is valid for any critical depth channel control; equating (39) and (40) one obtains for the specific case of a rectangular control section again the Ippen-equation (26).
From (38) and (40) follows an expression for the critical depth D_c:

$$D_c = \frac{2}{3} H_o \left(1 + \frac{1}{3}\varepsilon - \frac{4\delta_d}{3B} - \frac{\delta_d}{H_o}\right) < \frac{2}{3} H_o \qquad \ldots\ldots\ldots (41)$$

By a procedure similar to the equating of (39) and (40) Kalkwijk {6} succeeded in deriving a discharge relationship for any arbitrary shape with a correction for the boundary layer development, such as for instance for triangular cross section with top angle ϕ^o:

$$Q = \left(\frac{4}{5}\right)^{5/2} \tfrac{1}{2}(2g)^{\frac{1}{2}} \left(H_o - \frac{1}{\sin\left(\frac{\phi}{2}\right)} \cdot \delta_d\right)^{5/2} \cdot \operatorname{tg}\left(\frac{\phi}{2}\right) \qquad \ldots\ldots\ldots (42)$$

Although the resulting discharge relationship of rectangular cross section is in accordance with equation (26), the expression for the critical depth D_c (41) is different from the expression (24a), for which no reason can be found.
On the other hand Harrison {14} shows that a slightly different concept of deriving a discharge relationship, also results in $D_c < \frac{2}{3} H_o$. However, the theoretical determination of the critical depth is of minor importance in this study, since it does not affect the earlier produced discharge relationships, and it will therefore not be further discussed.

2.2.4. Theoretical and experimental values of the discharge coefficient C_D

Hall {3} applied the Ippen-equation (26) in the case of a sharp edged broad-crested weir. He made assumptions for the place and height of the so-called "separation bubble", which occurs just after the upstream edge of the weir-crest and he derived the following expression:

$$(1 - C_D) = 0.069\left(\frac{L}{H_o} - 1.0 + 2.84\, R_{H_o}^{0.25}\right)^{0.8} \cdot R_{H_o}^{-0.2}$$

$$R_{H_o} = \frac{U \cdot H_o}{\nu}$$

Although in principle the Ippen-equation does not allow for separation bubbles

(separation of flow), Hall observed that the computed values of C_D fit in very well with the experimental C_D-values.

On the basis of experimental data taken from Bazin, Woodburn and others, Harrison {4} compared observed C_D-values with computed values by application of the Ippen-equation:

$$C_D = \frac{Q}{(\frac{2}{3})^{3/2} \cdot g^{\frac{1}{2}} \cdot B \cdot H_o^{3/2}} = (1 - 2\frac{\delta_d}{B})(1 - \frac{\delta_d}{H_o})^{3/2} \quad \ldots\ldots (44)$$

In order to obtain the values of δ_d, Harrison used the theoretical values of the relative boundary layer displacement thickness on a flat plate {5}. Here too, the agreement between experiment and theory was satisfactory, as for example can be seen in Fig. 7. Harrison observed significant disagreement only between computed and measured C_D-values for heigh H_o/L values (depending on the ratio R/H_o). The exact determination of δ_d causes a problem, since the transition Reynolds number R_t is not known. However, the maximum error in C_D, which is introduced with R_t ranging between 3.10^5 and 10^6 amounts to 1%, as an average, {4} and {14}.

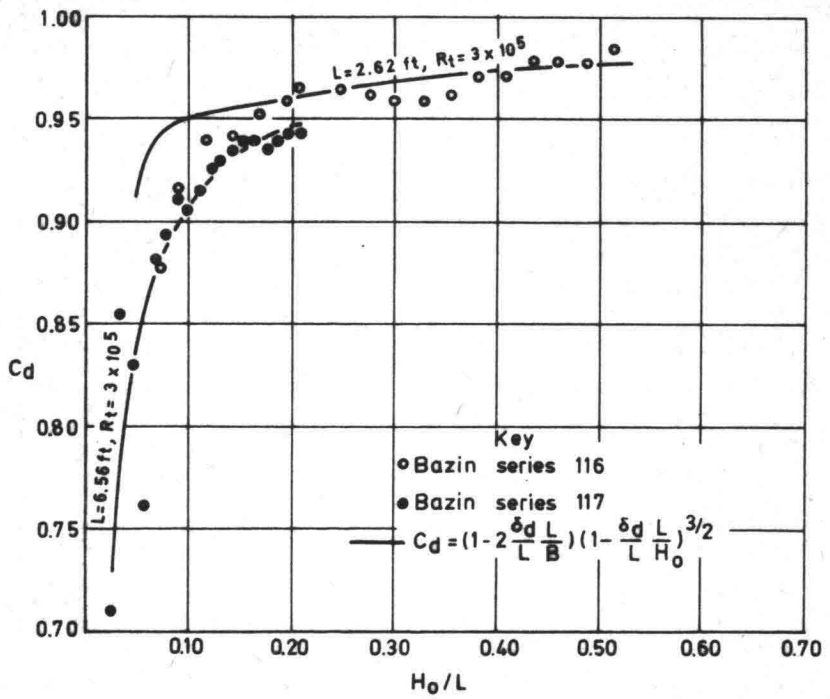

Fig. 7 Discharge coefficient data: Bazin
(A.J.M. Harrison 1968)

Recently Lakshmana Rao et.al. {24} designed a new type of streamlined broad-crested weir without a horizontal crest. The theoretically obtained C_D-values, which were corrected for the boundary layer growth on the weir, were compared with experimental observations and the agreement was found to be satisfactory.

2.2.5. Curvature effects of streamlines

One of the starting-points when developing a discharge relationship was the assumption of rectilinearity of parallel streamlines over the crest. It is obvious that this assumption does not hold for great values of the relative specific head H_o/L.
BSI publications {10} show that C_D does not remain constant if $H_o/L > 0.33$, but will increase as a result of the increasing curvilinearity of the streamlines over the weir, with consequent pressure reduction. Harrison stated that the assumption of rectilinear and parallel flow can only produce an error of about 0.5% in the computed discharge. In general one may expect that streamlined weir shapes possess heigher discharge coefficients as a consequence of lower drag characteristics and curvilinearity of flow.

Besides the curvature, the streamlines over the weir will converge slightly towards the downstream end of the crest, with a consequent increase of velocity in the direction of flow. The positive velocity gradient ($\frac{\partial u}{\partial x} > 0$) represses the perturbations (instability) with in the boundary layer, which prevent the boundary layer to develop as fast as on a flat plate in an infinite fluid ($\frac{\partial u}{\partial x} = 0$). These phenomena were already recognized by Nikuradse {17} and confirmed in experiments by Delleur {2}.

Finally, the curvature of flow at the upstream edge of the weir (contraction of streamlines), which is influenced by the radius R of the rounded-off nose, influences the C_D-values (pressure reduction). According to Harrison {4} C_D has to be a function of the dimensionless ratio R/H_o. Assuming that the radius of the curvature of a streamline varies linearly with the depth at the beginning of the horizontal crest, Jaeger {22} derived for two-dimensional irrotational flow:

$$\frac{du}{dy} = - \frac{u}{R + My}$$

in which u = velocity along the streamline at elevation y, M = a constant for any y (for broad-crested weir ≈ 6) which is a measure of the curvature of flow and:

$$C_D \left(\frac{2}{3}\right)^{3/2} \cdot g^{\frac{1}{2}} \cdot H_o^{3/2} = \frac{\{2g(H_o - h_o)\}^{\frac{1}{2}}}{M - 1} \{R + Mh_o - (R + Mh_o)^{\frac{1}{2}} \cdot R^{1-1/M}\} \quad \ldots\ (48)$$

in which h_o = water depth at the beginning of the horizontal crest (see Fig. 6).

It can be proved {4} that C_D decreases with increasing values of R/H_o for a constant value of L/H_o.

In general one can state that as regards influencing the discharge coefficient curvature of flow over the weir can be a more predominant factor than the viscous effects (form resistance).

2.2.6. Scale effects of modelling and dimensional analysis

If the flow characteristics of a measuring device are being determined in a laboratory scale model, one has to meet the requirement of dynamical similarity in order to allow for scale-effects. Neglecting the viscous effects as compared to gravity and pressure forces (forces of inertia), the requirement becomes:

$$\frac{(\rho g L^3)_{pr}}{(\rho g l^3)_m} = \frac{(\rho L^4 T^{-2})_{pr}}{(\rho l^4 t^{-2})_m}$$

(in which the suffixes pr and m denote prototype and model respectively), or the equality of the Froude number:

$$\left\{\frac{U}{(gL)^{\frac{1}{2}}}\right\}_{pr} = \left\{\frac{u}{(gl)^{\frac{1}{2}}}\right\}_m \qquad \ldots\ldots\ldots (49)$$

In this particular study the viscous effects may not be neglected (friction forces, boundary layer!), so that in fact the dynamic similarity of model and prototype also requires the equality of Reynolds numbers. In addition, only laminar or transition boundary layers are formed in the laboratory scale models, which makes it difficult to predict the influence of wall roughness in the prototypes. (Field devices operate at higher values of R_t than can be covered in laboratory installations!).

In order to overcome these difficulties and to adjust for boundary layer effects in scale models, one can introduce a new requirement of similarity:

$$\left(\frac{\delta_d}{x}\right)_m = \left(\frac{\delta_d}{x}\right)_{pr} \qquad \ldots\ldots\ldots (50)$$

At the same time one has to fulfil the requirement of dynamic similarity (49) and having a scale ratio of length, $^1/L = N$, it follows for the length Reynolds number which has to be persued in the model:

$$(R_x)_m = N^{3/2}(R_x)_{pr} \qquad \ldots\ldots\ldots (51)$$

For $(R_x)_m < 3.10^5$ the wall roughness has no influence on the boundary layer development. If $(R_x)_m > 3.10^5$, a combination of requirement (50) and (51) yields a value for the relative roughness $(\frac{x}{k})_m$, which can easily be seen in the $\frac{\delta_d}{x}$ - curves (Fig. 5). The curve which passes through the point of intersection of the line $(\frac{\delta_d}{x})_m$ = constant and $(R_x)_m$ = constant defines the value of $(\frac{x}{k})_m$ and as a consequence the equivalent roughness height k, which has to be applied in the model. This type of laws of scale is also applicable in models of closed conduits (Harp diagram of Nikuradse!)

Since C_D is a function of the relative boundary layer displacement $\delta_d/x = f(R_x, \frac{x}{k})$, one may expect C_D to be a function of some dimensionless groups.
Dimensional analysis involving the use of the Pi - theorem yields the following result:

$$Q = f(H_o, g, \mu, \rho, B, L, k) = f(H_o^a, g^b, \mu^c, \rho^d, B^e, L^f, k^g)$$

$$3 = a + b - c - 3d + e + f + g$$

$$-1 = -2b - c$$

$$0 = c + d$$

Solving these equations yields:

$$\frac{Q}{H_o^{5/2} \cdot g^{\frac{1}{2}}} = \Psi\{(\frac{H_o^{3/2} \cdot g^{\frac{1}{2}}}{\nu}), (\frac{L}{H_o}), (\frac{B}{H_o}), (\frac{k}{H_o})\}$$

The leftside of this expression can be rewritten as follows:

$$C_D \cdot \frac{H_o}{B} = \Psi\{R_g, (\frac{L}{H_o}), (\frac{B}{H_o}), (\frac{k}{H_o})\} \qquad \ldots\ldots\ldots (52)$$

from which can be seen that C_D is a function of some dimensionless groups, in which R_g may be considered as a particular Reynolds number. It is obvious that one can perform the dimensional analysis with other groups of variables and add, for instance U, P and R.

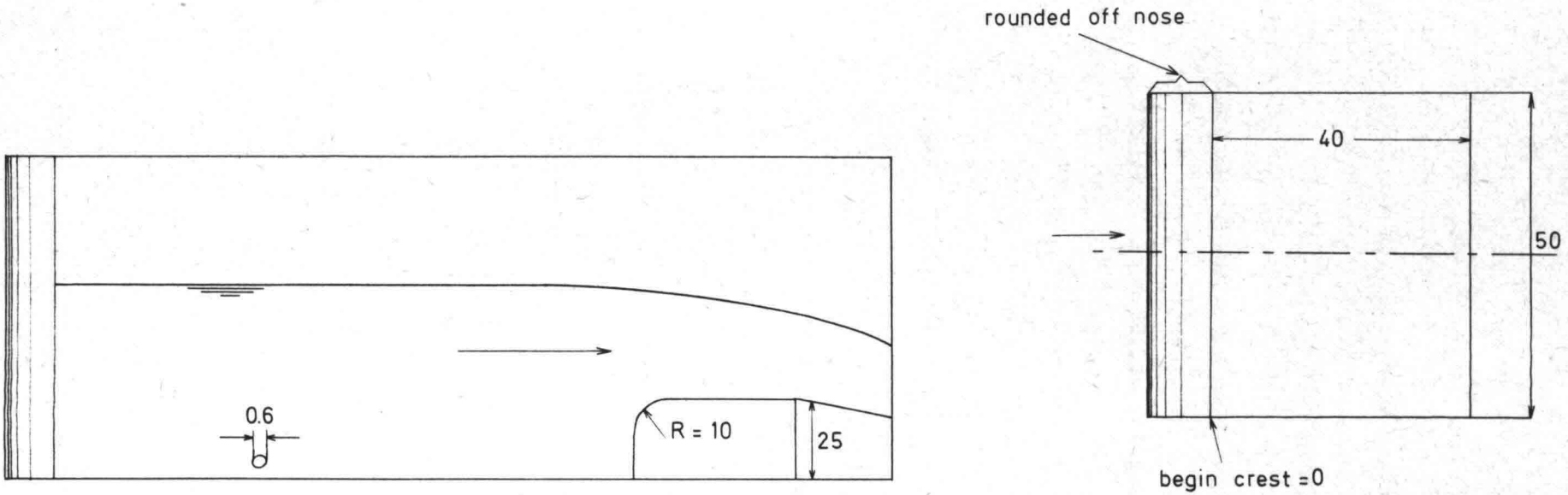

FIG. 8 Definition drawing of the broad-crested weir model
(L = 40 cm)
(measures in cm)

3. EXPERIMENTAL SET-UP AND RESULTS

3.1. Description of experimental set-up and measuring equipment

The experimental set-up consisted of two consecutive models of rectangular broad-crested weirs with a weir-height P = 25 cm, which were both placed in an approach flume of 50 cm width and 180 cm length (see Fig. 8).
The weir-tables were made of stainless steel and had a length of 40 cm and 120 cm respectively. Both had a rounded off nose with radius R = 10 cm. The discharges were measured with a volumetricaly calibrated V-notch, while the velocity profiles were measured with a so-called "wall-Pitot" tube, which was attached to a sledge, moving along a rail in the flow direction and perpendicular to it. The dynamic and static tube were both connected to the legs of a sensitive differential membrane manometer (d.m.m.) for measurement with a maximum reach of Δp = 100 cm column. The signal of the d.m.m. was electronically amplified and recorded with a volt-meter. Since this d.m.m. reacts very quickly to small changes in pressure due to turbulance in flow, it proved necessary to filter the electrical signal of the d.m.m. in order to reduce the fluctuations in registration. It was possible to improve measurement recordings during the experiments and reference is made to Note Nr. 23 {9}.
The local velocity at time t in a turbulent flow may be written as:

$$u_t = \bar{u} + u'_t \qquad \ldots\ldots\ldots (53)$$

in which $\bar{u}$ = the mean velocity and u'_t = the deviation of the mean velocity at time t. The electronical recording equipment reproduces the mean velocity over a differential time of either 10 or 100 seconds in percentage of the maximum velocity, which is computed by:

$$u_{max} = C(2g\Delta p_{max})^{\frac{1}{2}} \qquad \ldots\ldots\ldots (54)$$

in which g = 9.80665 (m/sec^2), Δp_{max} = maximum pressure difference which can be registrated by the d.m.m. and C = energy loss correction factor of the "wall-Pitot" tube.
A correction for the energy losses of the dynamic tube, which becomes particularly significant for low velocities, has to be applied to the "wall-Pitot" tube. For a detailed description reference is made to Note Nr. 16 {8}. In this Note

measured velocity profiles:

Q (l/sec)	C_{av}
100 and 80	1.000
70 and 65	1.010
50 and 25	1.035

Table II: Applied average correction factors for "wall-Pitot" tube

The accuracy of the velocity measurement is mainly affected by methodological errors (e.g. improper setting of the tubes) and sampling errors. The latter amount to $\pm$ 0.5% of the maximum pressure difference (and thus maximum velocity) for measurements on the short weir table (L = 40 cm), while for the long weir table (L = 120 cm) the accuracy of measurement could be increased upto $\pm$ 0.05%.

In principle it is possible to analyse the velocity measurements by means of a graphical method of regression i.e. a graphically fitted curve through the observation points, minimizing deviations from this line. Since this method does not give an accurate and objective determination of the parameters, and is in addition very time consuming, an attempt has been made to find a model of regression, which would enable a convenient analytical method of determining the parameters of the model (analytical curve fitting). The knowledge of the analytical or emperial formulas for velocity distribution forms the basis for the desired model of regression.

In the hydraulics of open channels {24} some semi-analytical resistance equations for the velocity distribution of turbulent flow along either hydraulic smooth or hydraulic rough boundaries are known. The most common equation is the general logarithmic formula of Prandtl-von Karman:

$$\frac{u}{u_*} = \frac{2.303}{\kappa} \log \left(\frac{y}{y'}\right) \qquad \ldots\ldots\ldots (56)$$

in which y = the distance above the boundary, y' = the distance of the point of zero velocity above the boundary and κ = von Karman turbulence constant ($\approx$0.4). Using empirically determined expressions for y' (Nikuradse) in equation (56), yields for smooth boundaries:

it is shown the "wall-Pitot" tube indicates velocities which are on an average 2% lower than those measured with a standard Pitot tube. In order to obtain some numerical values of C, which could be applied in this particular study, some complete series of velocity profiles were measured in a cross section on the weir-crest (see also Fig. 21). The average value of C is computed as follows:

$$Q_{ad} = C_{av} \cdot \iint_A u\,dA \quad \text{and} \quad u = (2g\,\Delta p)^{\frac{1}{2}} \qquad \ldots\ldots\ldots (55)$$

in which Q_{ad} = the adjusted discharge rate in the laboratory installation and C_{av} = the average correction factor of the "wall-Pitot" tube.
The obtained results are shown in Table I:

Adjusted discharge rate (l/sec)	Length of weir crest	Discharge rate derived from velocity profiles	C_{av}
25	40 cm	23.9317	1.0427
50		48.6110	1.0278
65	120 cm	64.3835	1.0096
80		79.8554	1.0018
100		99.9594	1.0004

Table I: Calibration of "wall-Pitot" tube

Measurements of vertical pressure distributions above the crest were also performed in order to get an idea of the curvature of flow over the crest. There fore the static tube and a watercolumn with a constant head (reference level) were both connected with the legs of the d.m.m. and the local pressure can be found by substracting the counter pressure.

3.2. Results of measurements and data processing

For the measurement of the velocity distributions inside the boundary layer on the crest, the pressure fluctuations were averaged over a differential time of 100 sec. Outside the boundary layer, where the fluctuations were considerably less, an average over 10 sec. proved to be sufficient. Refering to the calibration as indicated in table I, the following corrections were applied to the

$$\frac{u}{u_*} = 5.75 \log \left(\frac{u_* . y}{\nu}\right) + 5.3 \qquad \ldots\ldots\ldots (57)$$

and for rough boundaries:

$$\frac{u}{u_*} = 5.75 \log \left(\frac{y}{k}\right) + 8.5 \qquad \ldots\ldots\ldots (58)$$

According to Harrison {5} the transition from hydraulic smooth to hydraulic rough boundaries occurs between the following limits:

$$3.3 < \frac{u_* . k}{\nu} < 41.3$$

An alternate commonly used law of velocity distribution for turbulent flow over a smooth boundary is the one-seventh power formula of Blasius:

$$\frac{u}{u_*} = 8.67 \left(\frac{u_* y}{\nu}\right)^{1/7} \qquad \left(R_e = \frac{\bar{u} . R_h}{\nu} < 10^5\right) \qquad \ldots\ldots\ldots (59)$$

Recently a new mathematical model for the velocity distribution in turbulent flow was developed by Willis {16} using an error function approximation to the kinematic eddy viscosity, i.e. the Gaussian distribution function:

$$\frac{y}{y_m} = \frac{1}{(2\pi)^{\frac{1}{2}}} \int_{-\infty}^{P_g} e^{-t^2/2} \, dt$$

in which y_m = depth of flow in which the velocity reaches maximum value ($U = u_m$) and P_g = Gaussian standard normal depth variable. The final form of the dimensionless velocity defect expression then becomes:

$$\frac{u_m - u}{u_*} = -\frac{1.668}{\kappa} \left\{P_g \left(1 - \frac{y}{y_m}\right) - \frac{1}{(2\pi)^{\frac{1}{2}}} e^{-P_g^2/2}\right\} \qquad \ldots\ldots\ldots (60)$$

Willis shows that expression (60) gives a good agreement between predicted and measured velocities all over the flow profile and is even more reliable than the Prandtl-von Karman model (56) for the inner region of the turbulent boundary layer ($y/y_m < 0.2$).

Although the previously mentioned equations (56, 59 and 60) have been utilized extensively for the analytical description of fluid flow phenomena, some uncertainties are encountered in applying these mathematical models to the particular case of weir flow.

First: the derivation of these models is based on the assumption of uniform flow.
Secondly: the mathematical models are applicable only to completely developed boundary layers (such as in open channels or closed conduits) or, as may be stated as well, only to velocity distributions within the boundary layer ($y_m = \delta$ and $U = u_m$).
Consequently, these mathematical models are not suitable to the analytical description of the whole of velocity distributions in the non-uniform flow with incompletely developed boundary layers of the broad-crested weir, but they may certainly be applied to the region within the boundary layers [16] (determination of boundary shear from velocity measurements).

By trial and error an appropriate model of regression was developed for this particular study, which (though without direct physical significance) might be considered as an extension of the Prandtl-von Karman model. This applied model of regression:

$$u(y) = a_o + a_1 \ln y + a_2 (\ln y)^2 + a_3 (\ln y)^3 = \sum_{i=o}^{3} a_i (\ln y)^i \quad \text{for } y > 0 \quad \ldots\ldots (70)$$

a_i = regression coefficient ($i = 0,1,2,3$)
seems adequate to fit most of the observed velocity profiles on the weir-crest.
In order to analytically determine the regression coefficients one has to minimize the sum of squares of departure S:

$$S = \sum_{j=1}^{N} \{u_j - \sum_{i=0}^{3} a_i (\ln y)^i\}^2 \quad \ldots\ldots\ldots (71)$$

(in which u_j = observed value of velocity and N = number of observed points) with respect to the coefficients a_i ($i = 0,1,2,3$).
The solution of the thus obtained set of four linear equations ($\frac{\partial S}{\partial a_i} = 0$) gives the required coefficients. This generating procedure could be executed by a CDC - 3200 computer, for which a FORTRAN IV program has been written, in which the linear equations are solved with the Gauss-elemination method (see Fig. 23).
The regression function (70) can in principle be enlarged to a higher degree polynomial function with respect to the reduced independent variable ln (y) (natural logarithm), but this does not seem to improve the goodness of fit, which can be measured and tested by the Chi-square test.

Some typical examples of velocity distribution function, which are fitted to the observed points of measurement, are shown in the figures 9 - 15; it can be

noticed that the regression model (70) permits an appropriate description of the velocity distributions, except in some cases where a region of serious divergence occurs near the free water surface (see for example Fig. 12 B). It can be seen from this example that the goodness of fit can "artificially" be improved by omitting some points from the region where high observation density occurs.

Regarding the velocity profiles it is obviously not always possible exactly to indicate the thickness of the boundary layer. However, an attempt is made to develop a general procedure to compute the boundary layer displacement thickness from the adjusted velocity distribution functions. In Fig. 14A for example, the regression function (70) proves to have a maximum value for y = 6.07 cm, which allows the following approximate computation of the displacement thickness:

$$\delta_d = \int_{y=o}^{y=D} (1 - \frac{u}{U})dy \approx \int_{y=o}^{y=\delta} (1 - \frac{u}{U})dy \approx \int_{y=o}^{y=6.07} (1 - \frac{u}{U})dy \quad \ldots\ldots\ldots (72)$$

The previously mentioned FORTRAN IV computer program (see Fig. 23) carries out the numerical integration of $\int_o^{\delta} udy$ according to the Simpson rule (with a maximum of 2^{11} integration intervals) and U follows from du/dy = 0 so that

$$\delta_d = \int_{y=o}^{y=6.07} \{1 - \frac{1}{U} \sum_{i=o}^{3} a_i (\ln y)^i\}dy \qquad y > o \qquad \ldots\ldots\ldots (73)$$

$$u(o) = o \text{ for } y = o$$

Since this velocity profile in Fig. 14A shows an almost constant velocity outside the boundary layer (rectilinearity of flow), the exact value of the upper integration limit in (73) does not seriously affect the outcome of the integral. A second error might occur because of the boundary condition u(0) = 0, which is added to the numerical integration procedure. This of course is not in accordance with regression model (70), since the function (u)y tends to negative infinity as y approaches zero, the intercept at the y-ordinate being very small ($< 10^{-2}$ cm). The thus introduced error proved to be less than -0.2% of δ_d. It may therefore be concluded that the proposed procedure of determining the boundary layer displacement thickness is sufficient for the purpose of this study. By a similar procedure of numerical integration (Simpson, FORTRAN IV), the average velocity $\bar{u}$ and the velocity coefficients α and β were also computed.

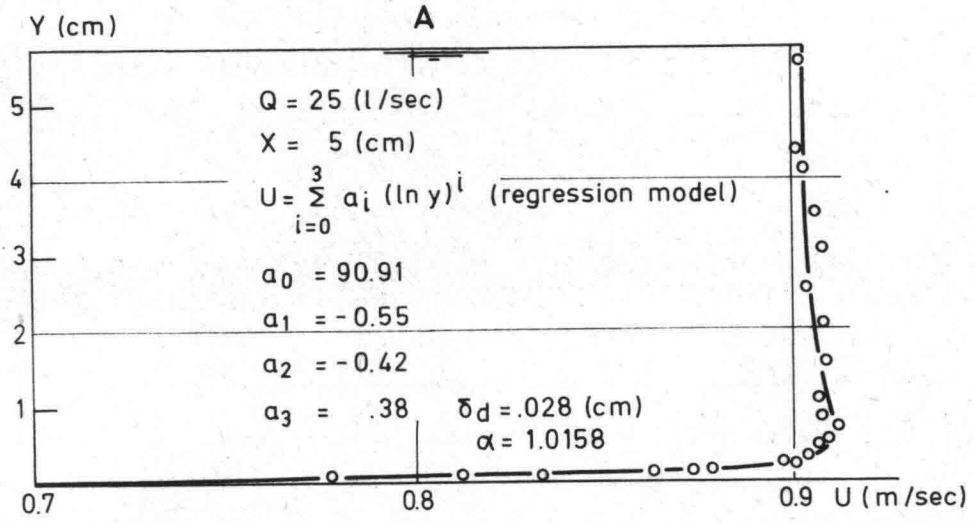

FIG. 9 Velocity distribution

L = 40 cm

o o o from direct measurement

—— regression line

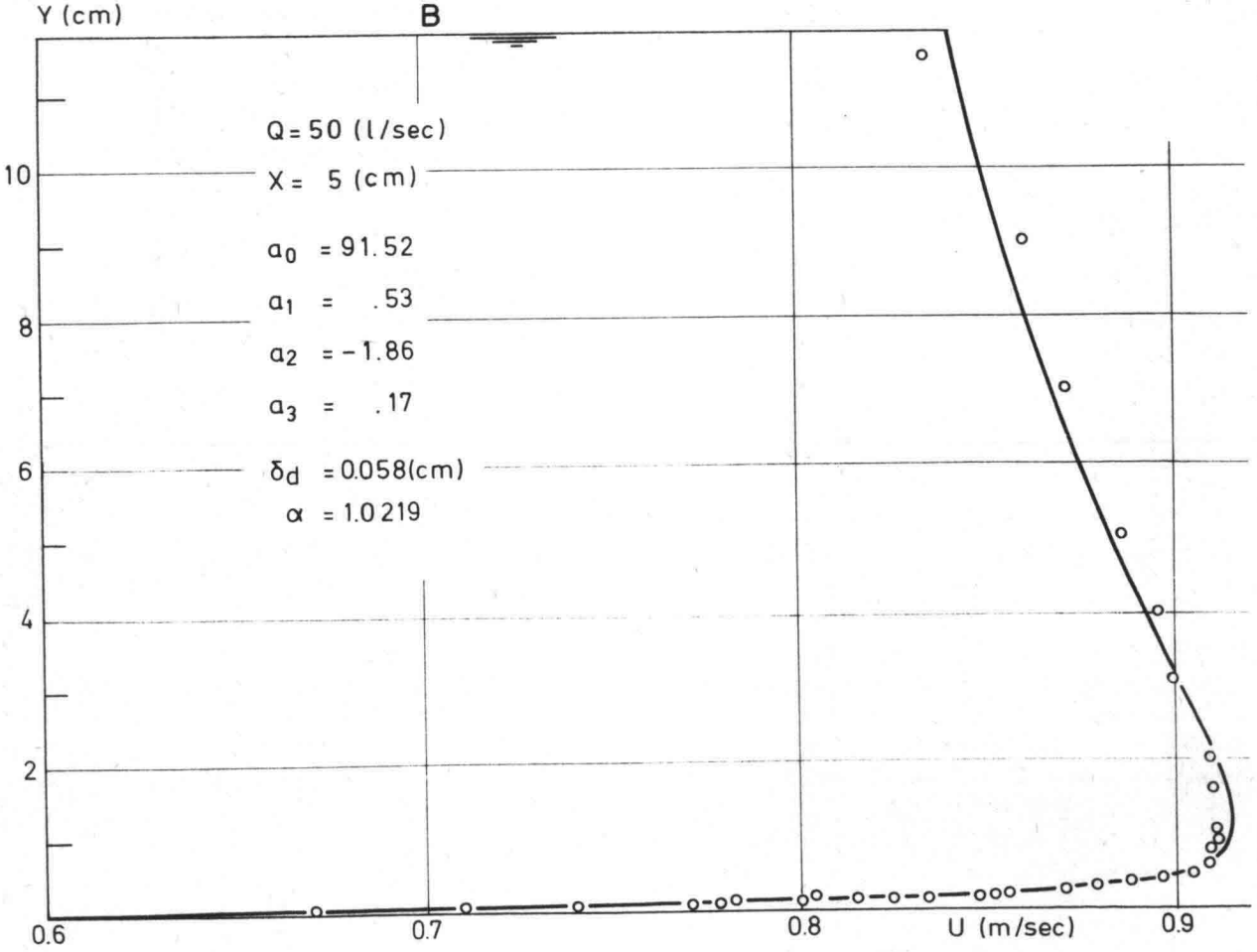

FIG. 10 Velocity distribution

L = 40 cm

ooo from direct measurement

—— regression line

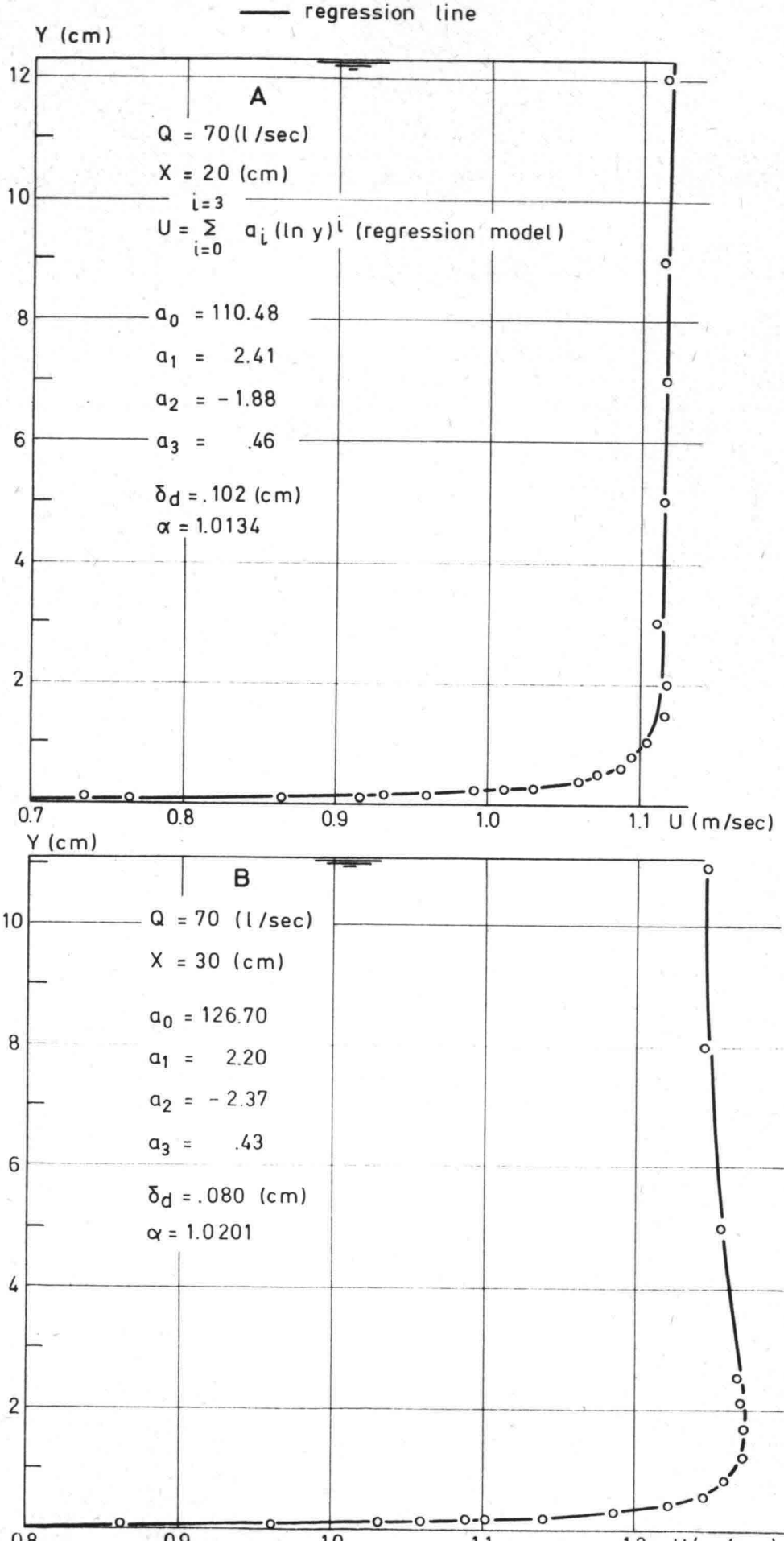

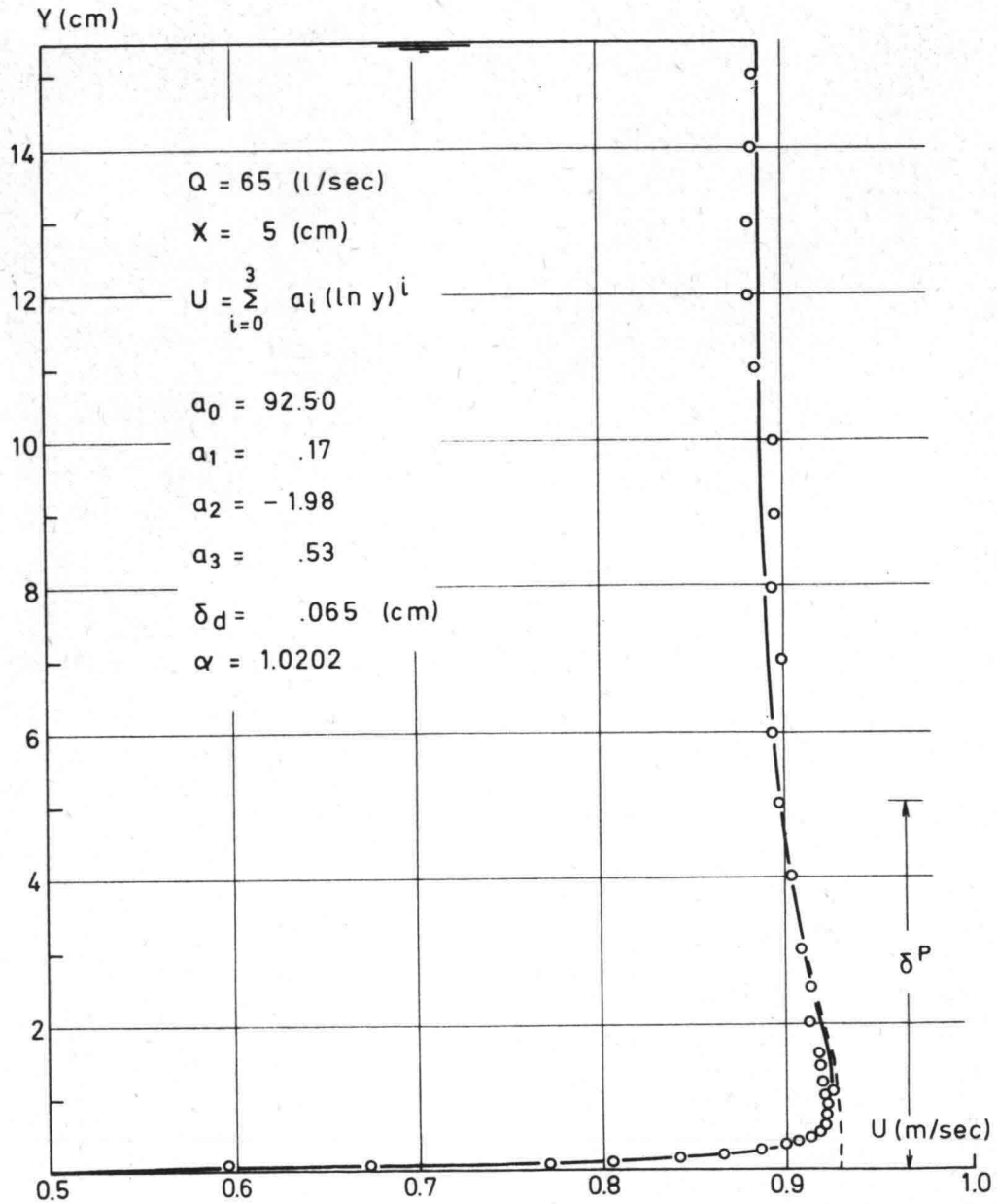

FIG. 11 Velocity distribution
L = 120 cm
ooo from direct measurement
—— regression line
– – undisturbed profile

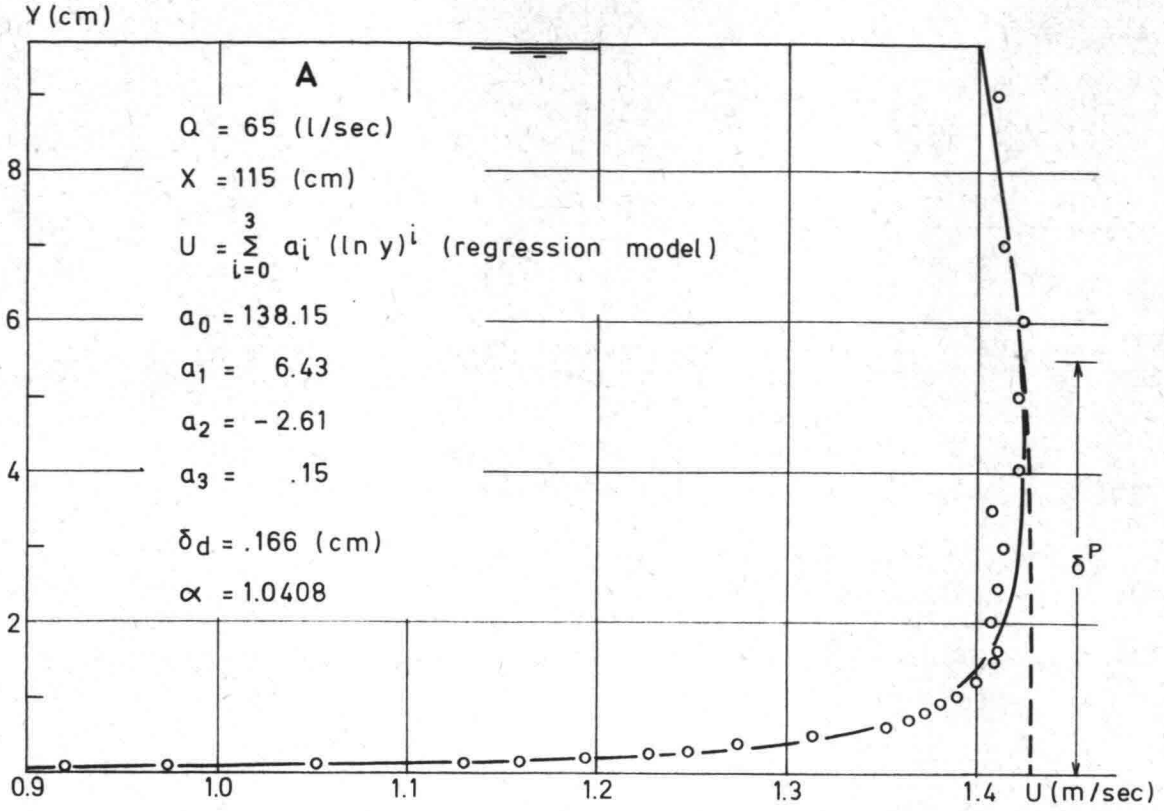

FIG. 12 Velocity distribution

o o o from direct measurement
—— regression line L = 120 cm
– – – undisturbed profile

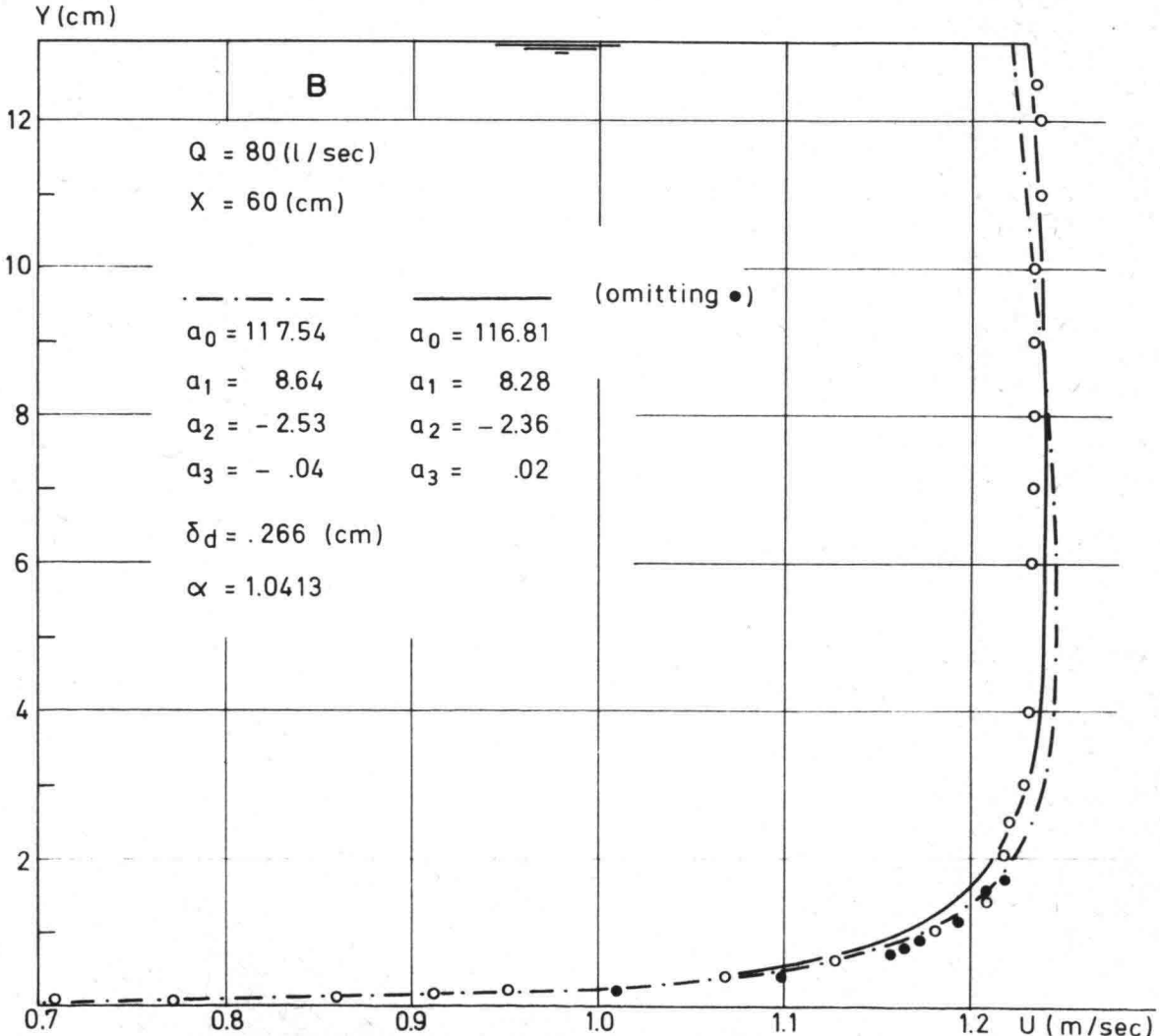

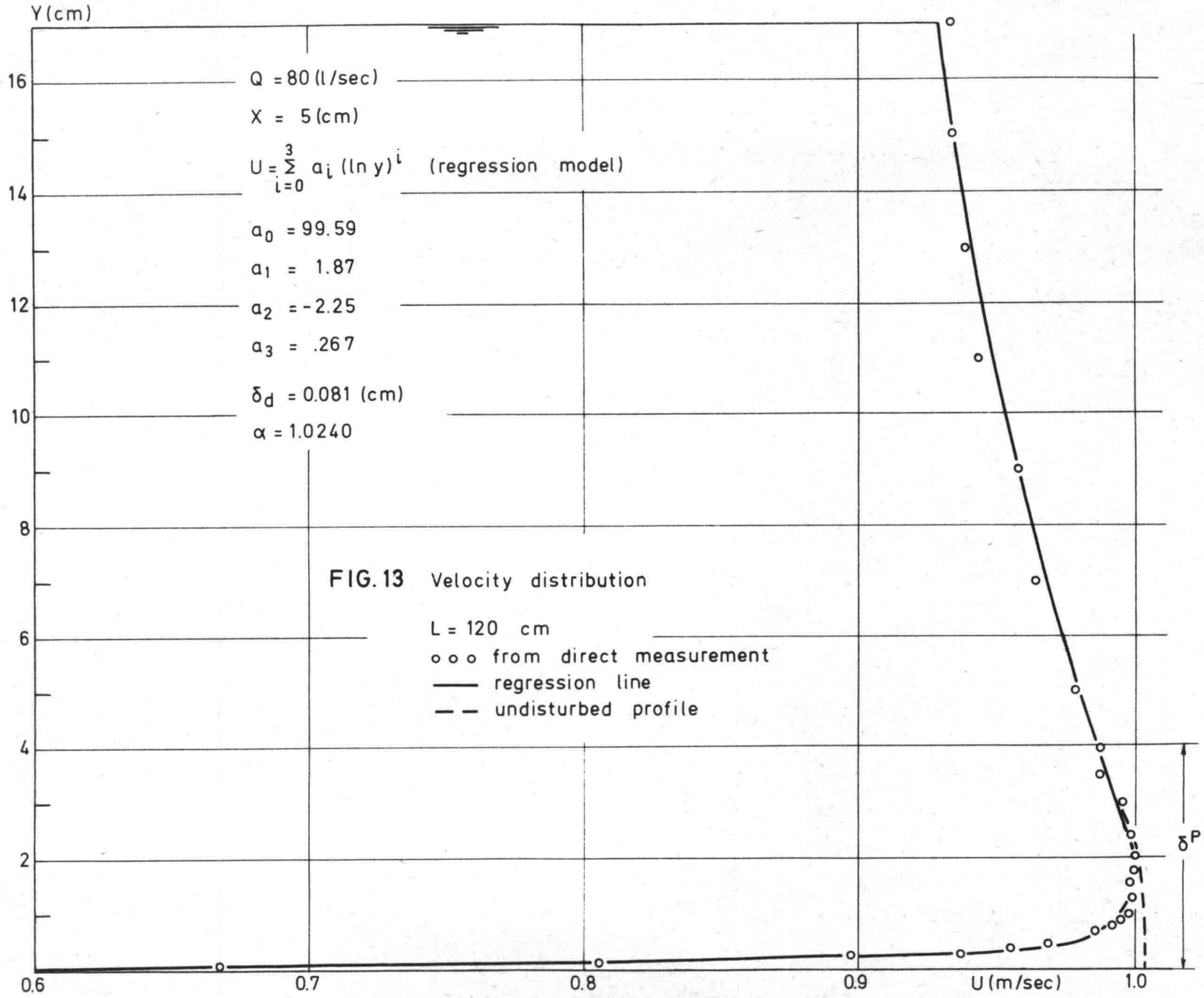

FIG. 13 Velocity distribution

L = 120 cm

o o o from direct measurement

—— regression line

– – undisturbed profile

FIG. 14 Velocity distribution

L = 120 cm

o o o from direct measurement

—— regression line

– – undisturbed profile

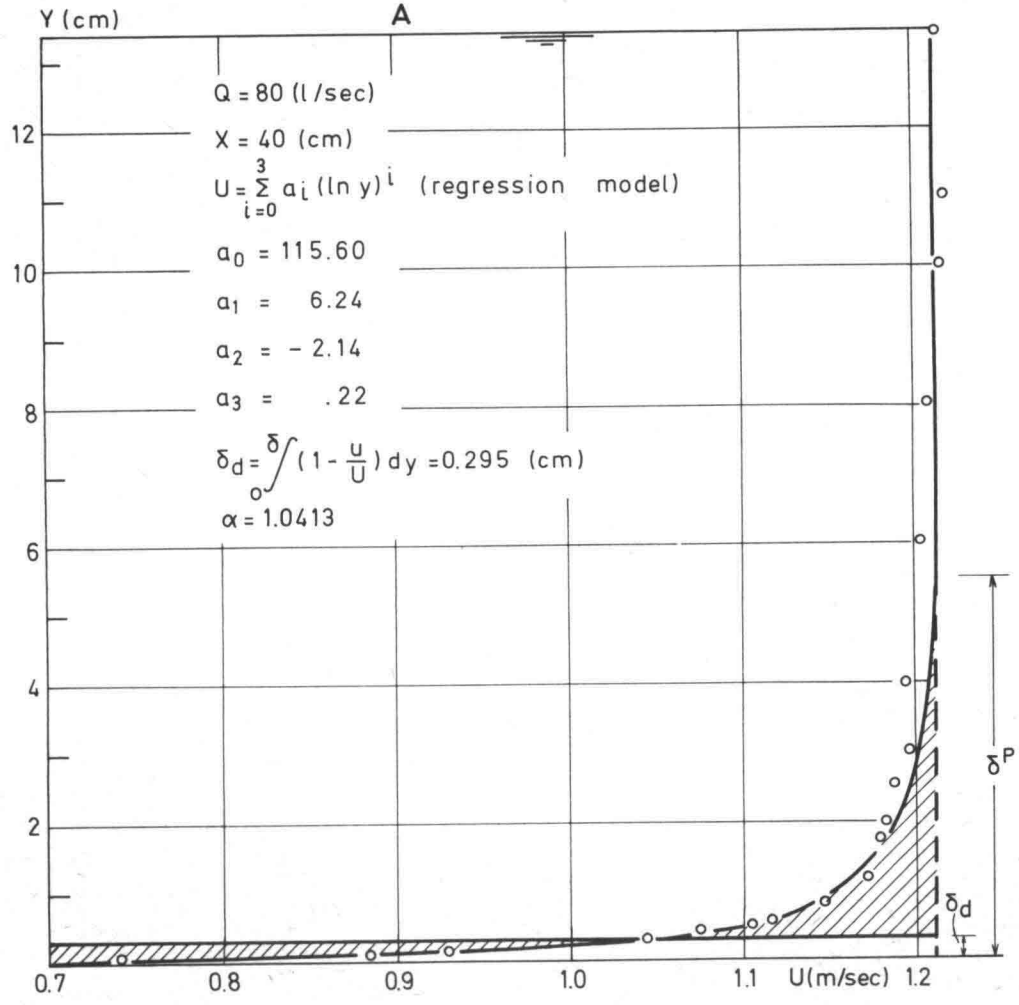

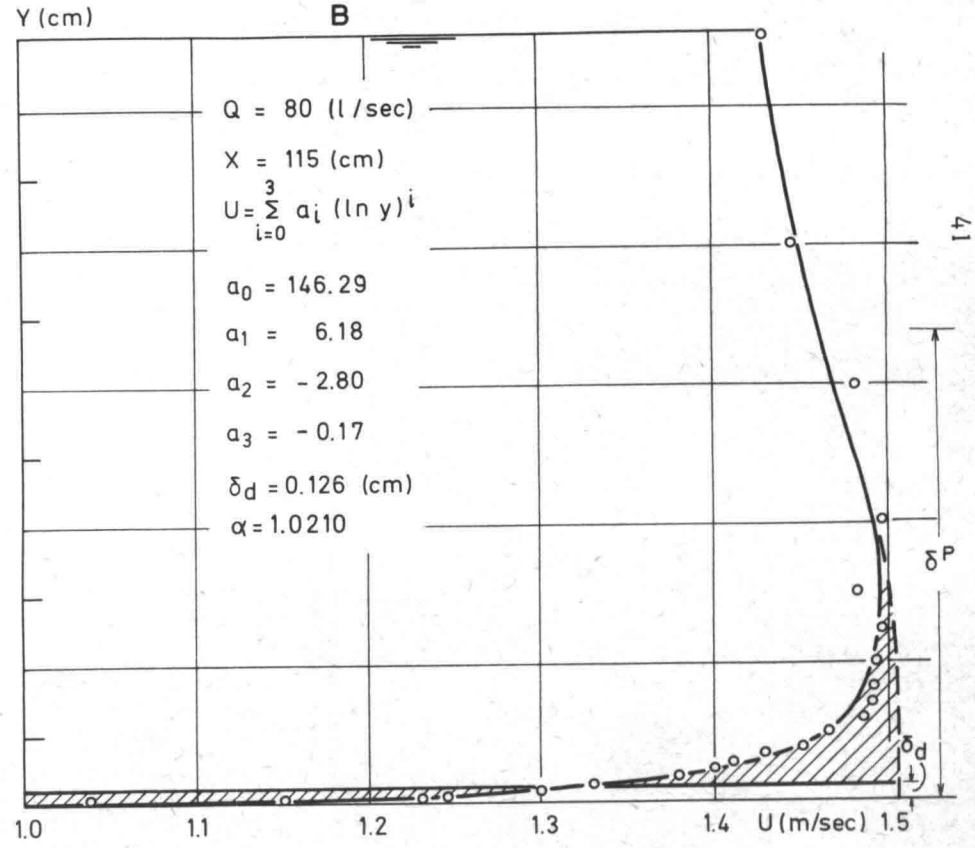

FIG. 15 Velocity distribution

L = 120 cm

ooo from direct measurement

—— regression line

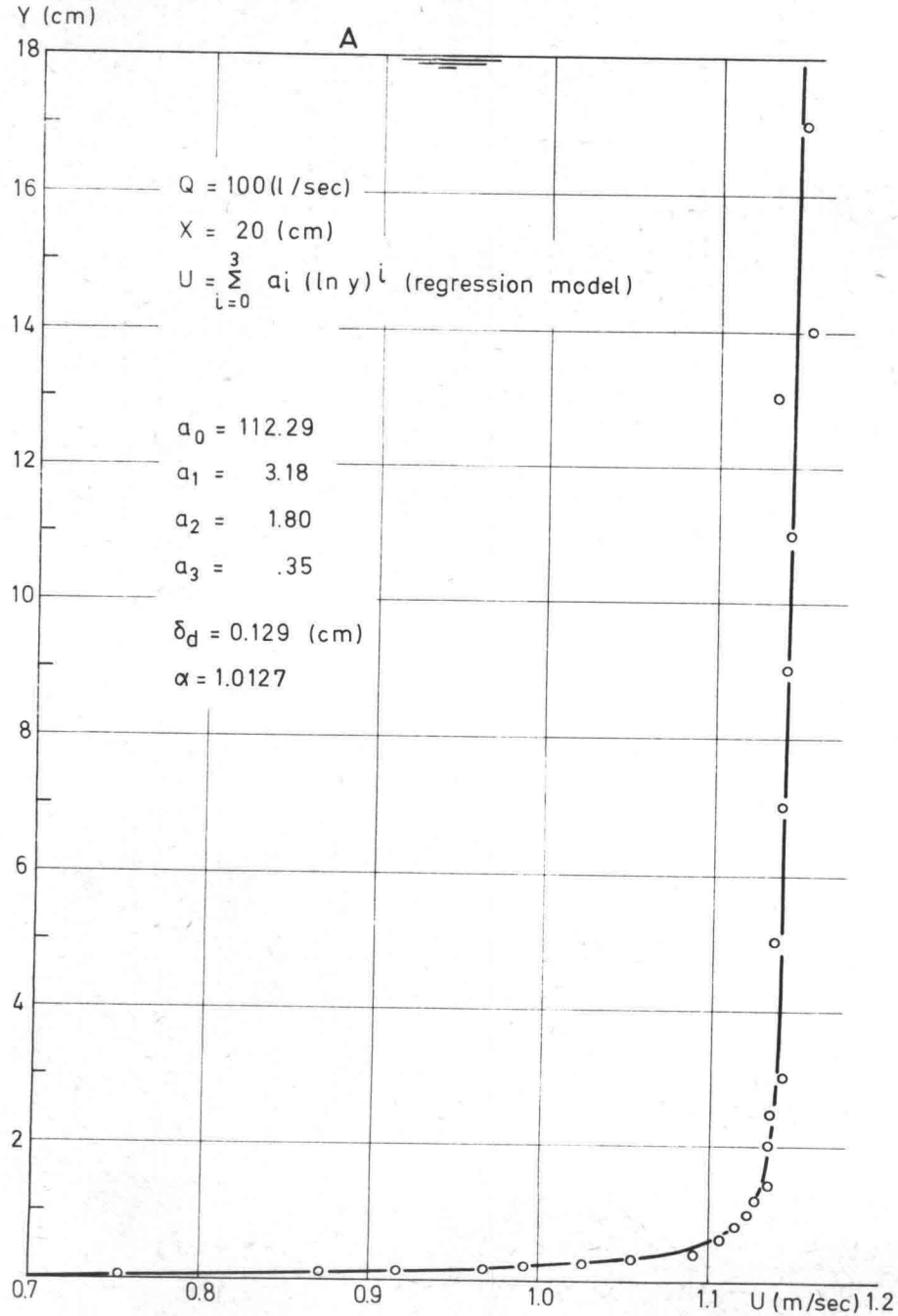

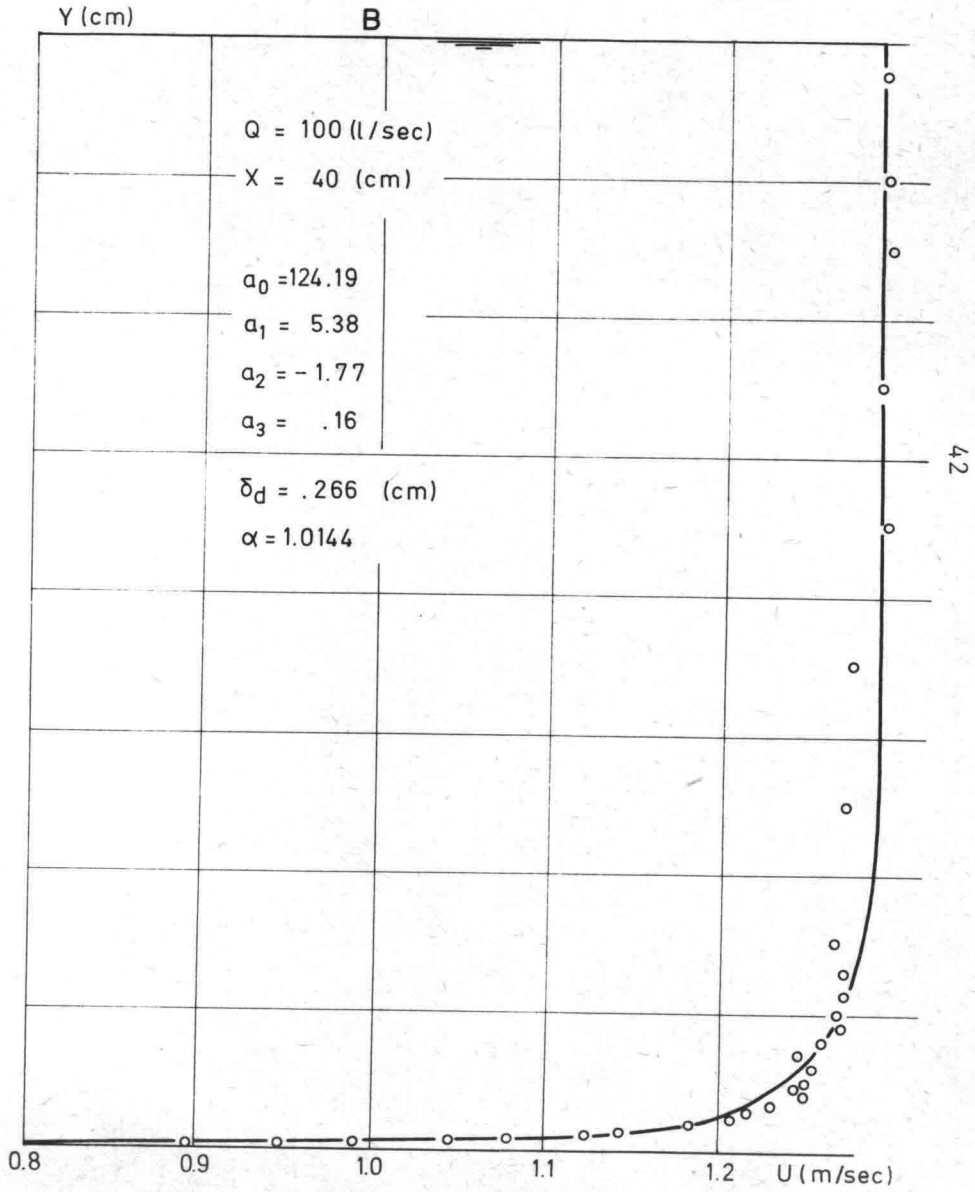

The velocity distribution profiles at the upstream and the downstream ends of the weir-crest however, do not show a constant velocity outside the boundary layer due to flow curvature (Fig. 9, 10B, 11, 12A, 13 and 14B). According to the definition, the boundary layer displacement thickness can be found by considering the velocity distribution without the viscous effects of the fluid (undisturbed potential flow). In the previous case of approximate rectilinearity of flow no problems are encountered, but if strong curvature of streamlines occurs it will be difficult to predict the undisturbed velocity profile (undisturbed here means: the imaginary velocity distribution which is not "disturbed" by friction effects of the boundary).

Therefore, we now consider the Euler-equation for two-dimensional flow in the vertical direction, normal to the streamlines {19}:

$$0 = -\frac{1}{\rho}\frac{\partial p}{\partial n} - g\frac{\partial y}{\partial n} - \frac{u^2}{r} \qquad \ldots\ldots\ldots (74)$$

in which p = local pressure, n = co-ordinate in the direction normal to the flow, y = elevation above the horizontal boundary and r = radius of curvature of streamline. The gradient of the piezometric head in the n-co-ordinate direction thus becomes:

$$\frac{\partial(\frac{P}{\rho g} + y)}{\partial n} = -\frac{u^2}{r} \qquad \ldots\ldots\ldots (75)$$

Since r tends to infinity near the boundary (crest), the piezometric head there becomes approximately constant and the tangent of the pressure distribution line consequently equals unity, which can be clearly seen in the observed pressure distribution profiles in the figures 16 an 17. From this, one can draw the conclusion, that rectilinearity of flow may be assumed to up a distance of 2 to 3 cm above the crest which means a practically vertical undisturbed velocity profile within this region, such as for instance is indicated in Fig. 14B. As a result of these considerations, the determination of the boundary layer thickness δ (in profiles where curvature of flow exists) has been approached by drawing a vertical tangent to the maximum value of the curve ($\frac{du}{dy} = 0$), where upon the displacement thickness δ_d has been computed by a procedure similar to the previously proposed one (73) (see also Fig. 12A and 13). It sometimes occurs that the shape of the obtained regression function (70) is such that the derivative of u(y) with respect to y becomes zero for $y > D$ (continues increasing for $y < D$).

FIG. 16 Pressure distribution

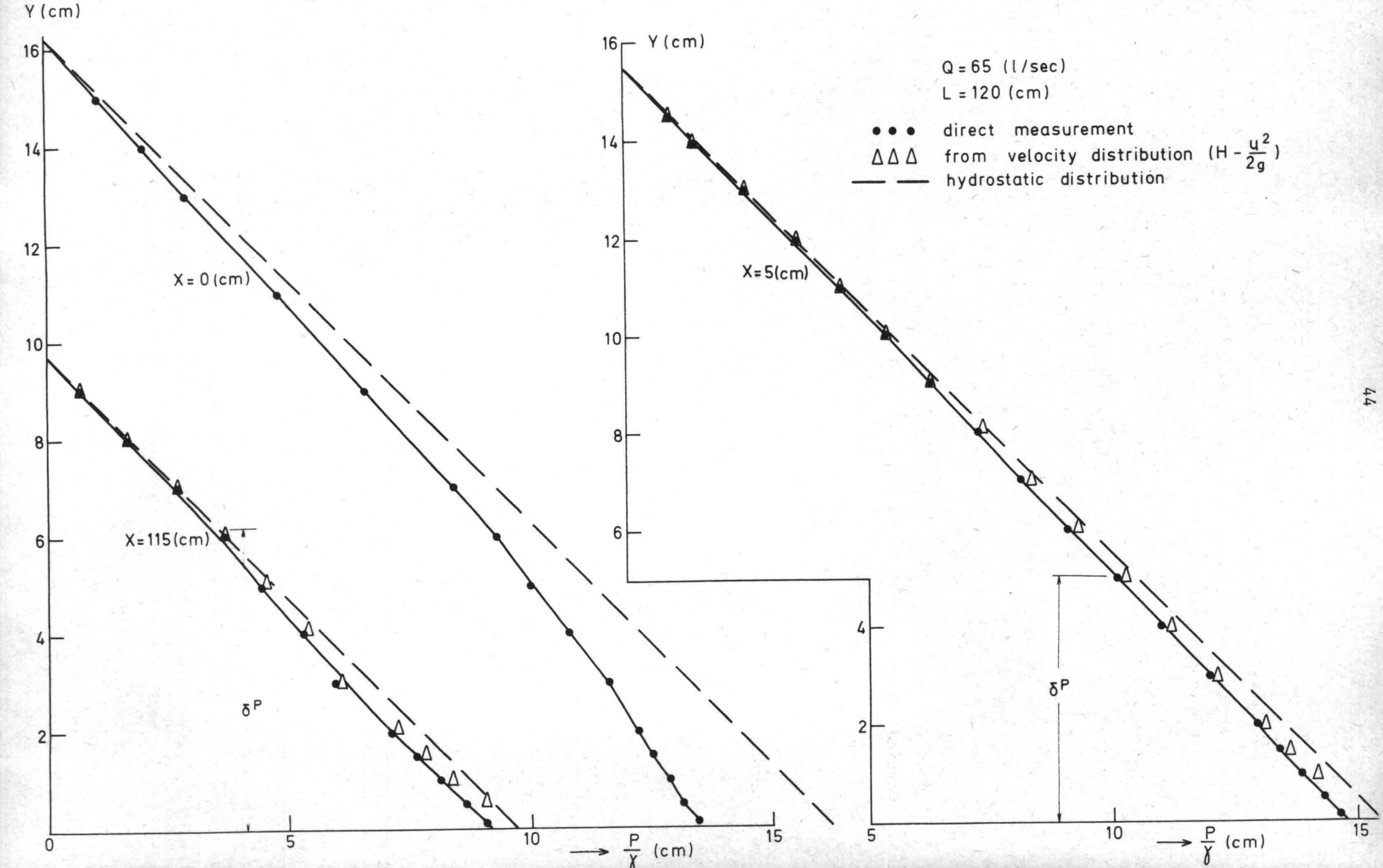

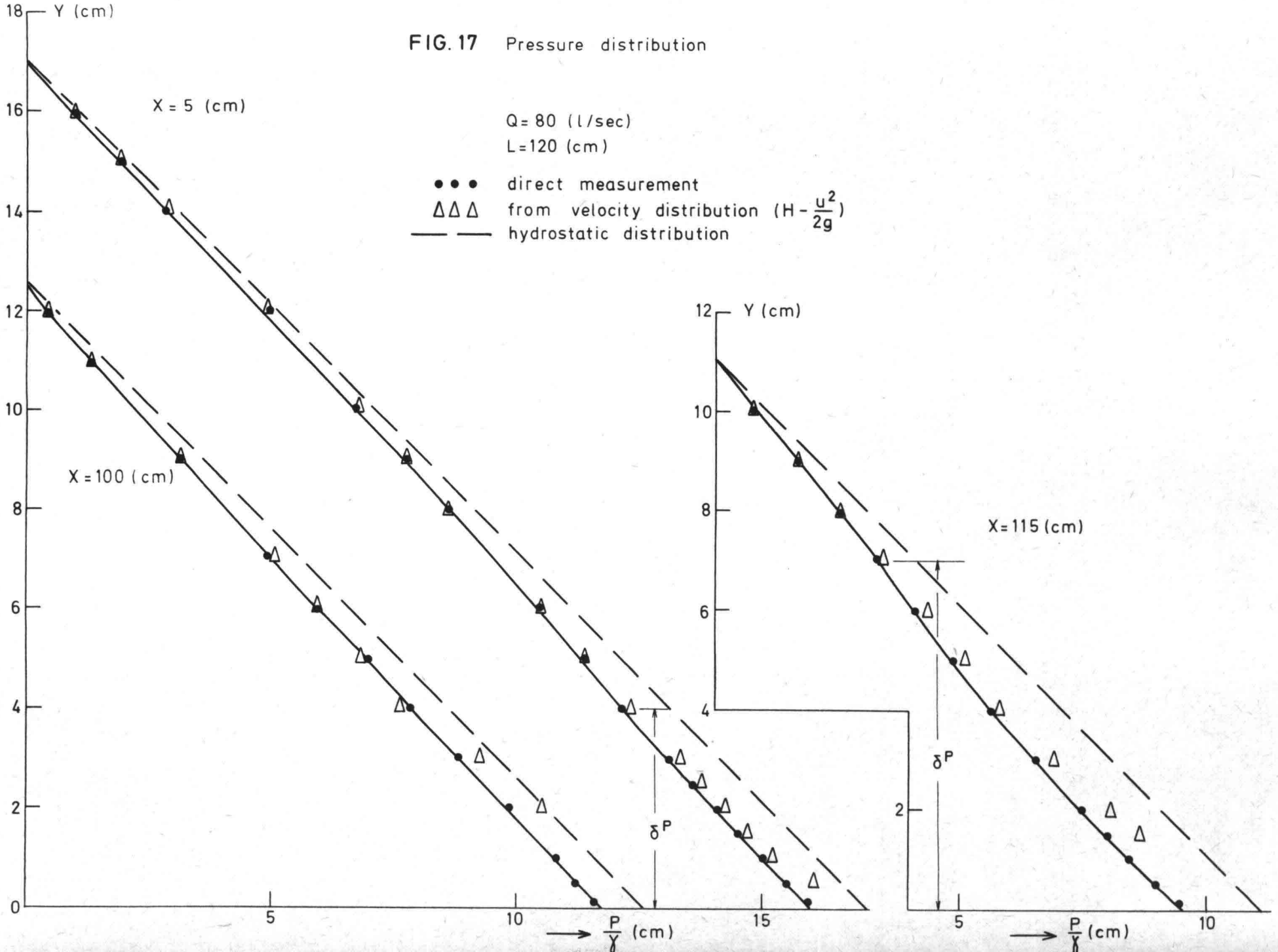

FIG. 17 Pressure distribution

Drawing, in those cases, (an example is given in Fig. 15A) a vertical tangent to the imaginary extreme value of u(y), has not much influence on the further computation of δ_d ($\frac{du}{dy} = 0$ for y = 20 cm in Fig. 15A).

It is possible to deduce the boundary layer thickness from the pressure distribution profiles. If hence, the flow is potential outside the boundary layer, then the total energy head H_p should be constant here:

$$H_p = \frac{p}{\rho g} + y + \frac{u^2}{2g} = \text{constant}$$

Comparing the direct measured pressure $(\frac{p}{\rho g})_d$ with the pressure derived from the adjusted velocity profiles $(H_p - \frac{u^2}{2g} - y)$, it can be stated for the region within the boundary layer (no potential flow):

$$(\frac{p}{\rho g})_d < (H_p - \frac{u^2}{2g} - y)$$

The region of divergence between the direct measured and the deduced pressures in the boundary layer, is roughly indicated in Fig. 16 and 17 by δ^p. The strong deviation from hydrostatic pressure (curvature of flow) at the beginning of the horizontal crest (x = 0) may also be noticed in Fig. 16.

Shear stress at the boundary along the axis of symmetry of the crest and around the side walls of several cross-sections was measured with a Preston tube, from which τ_o can be calculated as follows:

$$\log \frac{\tau_o d^2}{4\rho\nu^2} = -1.396 + \frac{7}{8} \log \frac{g\Delta p d^2}{4\nu}$$

with restrictions:

$$4.5 < \log \frac{g\Delta p d^2}{4\nu} < 6.5$$

in which the external diameter of the dynamic tube d = 3mm. For experimental data from the long weir-table (L = 120 cm) with adjusted discharge rates of 80 and 100 l/sec, τ_o was also deduced from the velocity distribution law of Prandtl-von Karman for smooth boundaries (57). The following physical magnitudes were used in the computations:

$\rho_{19^o} = 998.23 \ (kg/m^3)$

$\nu_{19^o} = 1.03 \ 10^{-6} \ (m^2/sec)$

The totality of processed experimental data is reproduced in the tables III A, B, C and IV A, B, C. On line 16 the corresponding value of the relative boundary layer displacement thickness δ_d/x on a flat plate in an infinite fluid is indicated, as computed by Harrison [5]. It was therefore assumed that the transition from a laminar to a turbulent boundary layer occurs for $R_t = 3.10^5$. This is justified according to Schlichting [11], since the flow in the approach flume is already preponderantly turbulent. The equivalent roughness height k was assumed to be 10^{-5}m, according to the average value for rolled stainless steel. On line 18 it shows the total energy head $H_p = D + \alpha \bar{U}^2/2g$, which in fact only has validity, when hydrostatic pressure exists. Finally, the C_D-value on line 19 follows from the application of the Ippen-equation (26), whereby δ_d is taken from line 13.

FIG. 18 Boundary layer displacement thickness and wall shear stresses

o——o wall shear stress τ_o (preston tube)
x——x Froude number F_R'

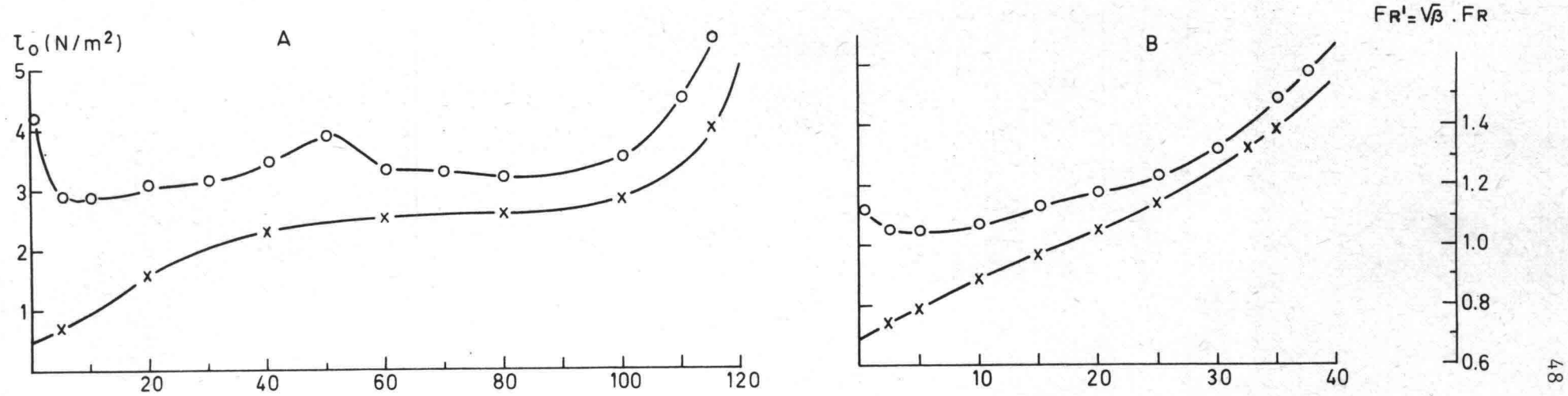

Δ——Δ boundary layer displacement thickness δ_d (from velocity distribution)
o o corresponding value of δ_d on a flat plate
x- - - -x floor pressure

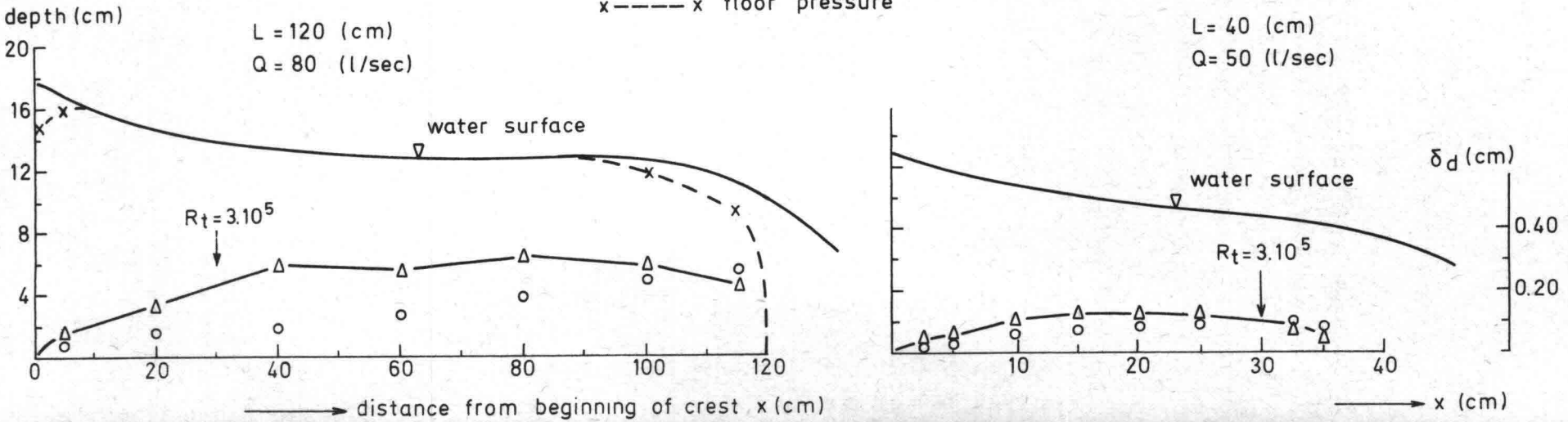

TABEL III A

Analysis of experimental data for short weir-table

L = 40 cm Q = 25 1/sec H_o/L = .2420

	X (cm)	5	15	20	25	30	35
2	D (cm)	7.06	6.08	5.87	5.74	5.46	5.14
3	A (cm^2)	353.0	304.0	293.5	287.0	273.0	257.0
4	$\bar{u}$ (cm/sec)	70.82	82.24	85.18	87.11	91.58	97.28
5	W (cm)	64.12	62.16	61.74	61.58	60.92	60.28
6	R_h (cm)	5.51	4.89	4.75	4.66	4.48	4.26
7	$R_e = \frac{\bar{u}, R_h}{\nu}$	$3.8\ 10^4$	$3.9\ 10^4$	$3.9\ 10^4$	$3.9\ 10^4$	$4.0\ 10^4$	$4.0\ 10^4$
8	U (cm/sec)	75.09	83.97	88.41	91.04	94.98	101.67
9	$R_x = \frac{U, x}{\nu}$	$3.65\ 10^4$	$1.22\ 10^5$	$1.72\ 10^5$	$2.21\ 10^5$	$2.77\ 10^5$	$3.45\ 10^5$
10	α	1.0158	1.0133	1.0199	1.0198	1.0202	1.0212
11	β	1.0102	1.0099	1.0099	1.0099	1.0099	1.0103
12	Fr^1 =	.861	1.076	1.134	1.172	1.263	1.384
	From measurement						
13	δ_d (cm)	.061	.040	.037	.28	.036	.032
14	δ_d/x	.0123	.0026	.00183	.00114	.00119	.00093
15	x/k	5000	15000	20000	25000	30000	35000
	Theor.						
16	δ_d/x	.0090	.0050	.0042	.0037	.0032	.0023
17	$\alpha \frac{\bar{U}^2}{2g}$ (cm)	2.60	3.49	3.77	3.95	4.36	4.93
18	H_p (cm)	9.66	9.57	9.64	9.69	9.82	10.07
19	C_D (Ippen)	.9881	.9923	.9929	.9945	.9931	.9937
20	τ_o (N/m^2) Preston tube	-	-	-	-	-	-
21	τ_o (N/m^2) velocity profile	-	-	-	-	-	-

TABEL III B

Analysis of experimental data for the short weir-table

L = 40 cm Q = 50 l/sec H_o/L = .3875

1	X (cm)	2.5	5	10	15	20	25	32.5	35
2	D (cm)	12.28	11.82	10.99	10.30	9.72	9.22	8.42	8.12
3	A (cm^2)	614.0	591.0	549.5	515.0	486.0	461.0	421.0	406.0
4	$\bar{u}$ (cm/sec)	81.43	84.60	90.99	97.09	102.88	108.46	118.76	123.15
5	W (cm)	74.46	73.64	71.98	70.60	69.44	68.44	66.84	66.24
6	R_h (cm)	8.25	8.03	7.63	7.29	7.00	6.74	6.30	6.13
7	$R_e = \frac{\bar{u}.R_h}{\nu}$	$6.52\ 10^4$	$6.60\ 10^4$	$6.74\ 10^4$	$6.87\ 10^4$	$6.99\ 10^4$	$7.09\ 10^4$	$7.26\ 10^4$	$7.33\ 10^4$
8	U (cm/sec)	92.54	91.56	94.93	99.93	105.35	111.21	123.02	131.99
9	$R_x = \frac{U.x}{\nu}$	$2.24\ 10^4$	$4.44\ 10^4$	$9.22\ 10^4$	$1.46\ 10^5$	$2.05\ 10^5$	$2.70\ 10^5$	$3.88\ 10^5$	$4.49\ 10^5$
10	α	1.0249	1.0219	1.0127	1.0144	1.0143	1.0140	1.0211	1.0210
11	β	1.0115	1.0105	1.0099	1.0029	1.0028	1.0026	1.0103	1.0103
12	Fr'	.751	.795	.884	.696	1.057	1.144	1.320	1.394
	from measurement								
13	δ_d (cm)	.048	.058	.104	.128	.126	.124	.093	.063
14	δ_d/x	.01919	.01165	.01165	.0104	.00853	.00495	.00285	.00179
15	x/k	2500	5000	10000	15000	20000	25000	32500	35000
	theor.								
16	δ_d/x	.0114	.00815	.0058	.0045	.0038	.0033	.0025	.0022
17	$\alpha \frac{\bar{U}^2}{2g}$ (cm)	3.47	3.73	4.10	4.87	5.47	6.08	7.34	7.89
18	H_p (cm)	15.75	15.55	15.09	15.17	15.29	15.30	15.76	16.01
19	C_D (Ippen)	.9934	.9920	.9857	.9825	.9827	.9830	.9873	.9914
20	Preston τ_o (N/m^2)	2.36	2.33	2.45	2.74	2.97	3.25	3.58	4.42
21	τ_o (N/m^2) velocity profile	-	-	-	-	-	-	-	-

TABEL III C

Analysis of experimental data for short weir-table

L = 40 cm Q = 70 l/sec H_o/L = .4788

1	X (cm)	2.5	5.0	10	15	20	25	30	35
2	D (cm)	15.45	14.97	14.09	13.22	12.34	11.69	11.10	10.20
3	A (cm^2)	772.5	748.5	704.5	661.0	6.17.0	584.0	555.0	510.0
4	$\bar{u}$ (cm/sec)	90.61	93.52	99.36	105.90	113.45	119.76	126.13	137.25
5	W (cm)	80.90	79.94	78.18	76.44	74.68	73.38	72.20	70.40
6	R_h (cm)	9.55	9.36	9.01	8.65	8.26	7.97	7.69	7.24
7	$R_e = \frac{\bar{u}.R_h}{\nu}$	$8.4\ 10^4$	$8.5\ 10^4$	$8.7\ 10^4$	$8.9\ 10^4$	$9.1\ 10^4$	$9.3\ 10^4$	$9.4\ 10^4$	$9.6\ 10^4$
8	U (cm/sec)	97.55	96.55	99.50	105.28	111.48	117.50	127.26	138.67
9	$R_x = \frac{U.x}{\nu}$	$2.37\ 10^4$	$4.68\ 10^4$	$9.66\ 10^4$	$1.53\ 10^5$	$2.16\ 10^5$	$2.85\ 10^5$	$3.71\ 10^5$	$4.71\ 10^5$
10	α	1.0256	1.0221	1.0198	1.0125	1.0134	1.0128	1.0201	1.0211
11	β	1.0117	1.0106	1.0098	1.0099	1.0023	1.0099	1.0099	1.0103
12	Fr'	.745	.780	.853	.939	1.033	1.130	1.221	1.386
from measurement									
13	δ_d (cm)	.065	.082	.077	.089	.102	.085	.080	.055
14	δ_d/x	.0261	.0164	.00766	.00597	.00511	.00340	.00265	.00156
15	x/k	2500	5000	10000	15000	20000	25000	30000	35000
theor.									
16	δ_d/x	.0110	.0079	.0057	.0045	.0037	.0032	.0026	.0021
17	$\alpha \frac{\bar{U}^2}{2g}$ (cm)	4.29	4.56	5.13	5.79	6.65	7.41	8.11	9.81
18	H_p (cm)	19.47	19.53	19.22	19.01	18.99	19.10	19.21	20.01
19	C_D (Ippen)	.9923	.9903	.9910	.9894	.9880	.9900	.9906	.9936
20	Preston τ_o(N/m^2)	-	-	-	-	-	-	-	-
21	τ_o(N/m^2) velocity profile	-	-	-	-	-	-	-	-

TABEL IV A

Analysis of experimental data for long weir-table

L = 120 cm Q = 65 l/sec H_o/L = .1551

1 X (cm)	5	20	40	60	80	100	115
2 D (cm)	15.44	12.45	11.50	11.47	11.45	11.18	9.69
3 A (cm^2)	772.0	622.5	575.0	573.5	572.5	559.0	484.5
4 $\bar{u}$ (cm/sec)	84.20	104.42	113.04	113.34	113.54	116.28	134.16
5 W (cm)	80.88	74.90	73.00	72.94	72.90	72.36	69.38
6 R_h (cm)	9.55	8.31	7.88	7.86	7.85	7.73	6.98
7 $R_e = \frac{\bar{u}.R_h}{\nu}$	$7.81\ 10^4$	$8.42\ 10^4$	$8.65\ 10^4$	$8.65\ 10^4$	$8.65\ 10^4$	$8.73\ 10^4$	$9.09\ 10^4$
8 U (cm/sec)	92.50	103.50	114.64	117.36	116.78	121.46	142.47
9 $R_x = \frac{U.x}{\nu}$	$4.50\ 10^4$	$2.02\ 10^5$	$4.45\ 10^5$	$6.84\ 10^5$	$9.07\ 10^5$	$1.18\ 10^6$	$1.59\ 10^6$
10 α	1.0202	1.0145	1.0405	1.0421	1.0420	1.0413	1.0408
11 β	1.0099	1.0029	1.0199	1.0205	1.0205	1.0203	1.0201
12 Fr'	.691	.949	1.085	1.091	1.098	1.133	1.404
from measurement							
13 δ_d (cm)	.065	.109	.177	.264	.259	.207	.166
14 δ_d/x	.01301	.00545	.00442	.00440	.0032	.00207	.00145
15 x/k	5000	20000	40000	60000	80000	100000	115000
theor.							
16 δ_d/x	.0081	.0037	.0021	.0023	.0023	.0024	.0024
17 $\alpha \frac{\bar{U}^2}{2g}$ (cm)	3.69	5.64	6.78	6.83	6.85	7.18	9.55
18 H_p (cm)	19.13	18.09	18.28	18.30	18.30	18.36	19.24
19 C_D (Ippen)	.9922	.9869	.9789	.9685	.9690	.9752	.9801
20 Preston τ_o(N/m^2)	2.58	2.93	3.09	2.84	2.58	3.01	4.79
21 τ_o(N/m^2) velocity profile	-	-	-	-	-	-	-

TABEL IV B

Analysis of experimental data for long weir-table

L = 120 cm Q = 80 l/sec H_o/L = .1746

1 X (cm)	5	20	40	60	80	100	115
2 D (cm)	17.01	14.79	13.39	13.07	12.95	12.55	11.03
3 A (cm^2)	850.5	739.5	669.5	653.5	647.5	627.5	551.5
4 $\bar{u}$ (cm/sec)	94.06	108.18	119.49	122.42	123.55	127.49	145.06
5 W (cm)	84.02	79.58	76.78	76.14	75.90	75.10	72.06
6 R_h (cm)	10.12	9.29	8.72	8.58	8.53	8.36	7.65
7 $R_e = \frac{\bar{u}.R_h}{\nu}$	$9.24\ 10^4$	$9.76\ 10^4$	$1.01\ 10^4$	$1.02\ 10^4$	$1.02\ 10^5$	$1.03\ 10^5$	$1.08\ 10^5$
8 U (cm/sec)	100.00	110.64	121.33	124.20	126.59	130.45	149.49
9 $R_x = \frac{U.x}{\nu}$	$4.85\ 10^4$	$2.15\ 10^5$	$4.71\ 10^5$	$7.23\ 10^5$	$9.83\ 10^5$	$1.26\ 10^6$	$1.67\ 10^6$
10 α	1.0213	1.0407	1.0409	1.0413	1.0424	1.0422	1.0210
11 β	1.0103	1.0200	1.0201	1.0203	1.0206	1.0205	1.0102
12 Fr'	.735	.917	1.064	1.103	1.119	1.173	1.409
from measurement							
13 δ_d (cm)	.081	.168	.295	.266	.315	.285	.126
14 δ_d/x	.0162	.0084	.0074	.0044	.0039	.0029	.0011
15 x/k	5000	20000	40000	60000	80000	100000	115000
theor.							
16 δ_d/x	.0078	.0037	.0022	.0023	.0024	.0024	.0024
17 $\alpha \frac{\bar{U}^2}{2g}$ (cm)	4.61	6.21	7.58	7.96	8.11	8.64	10.95
18 H_p (cm)	21.62	21.00	20.97	21.03	21.06	21.19	21.98
19 C_D (Ippen)	.9910	.9814	.9674	.9706	.9652	.9685	.9860
20 Preston τ_o (N/m^2)	2.90	3.02	3.46	3.32	3.20	3.55	5.53
21 τ_o (N/m^2) velocity profile	1.57	2.70	3.14	3.98	3.72	3.74	2.26

TABEL IV C

Analysis of experimental data for long weir-table

L = 120 cm Q = 100 l/sec H_o/L = .2024

1 X (cm)	5	20	40	60	80	100	115
2 D (cm)	19.99	17.62	15.76	15.05	14.73	14.14	12.60
3 A (cm^2)	999.5	881.0	788.0	752.5	736.5	707.0	630.0
4 $\bar{u}$ (cm/sec)	100.05	113.51	126.90	132.89	135.78	141.44	158.73
5 W (cm)	89.98	85.24	81.52	80.10	79.46	78.28	75.20
6 R_h (cm)	11.11	10.34	9.67	9.39	9.27	9.03	8.38
7 $R_e = \frac{\bar{u}.R_h}{\nu}$	$1.07\ 10^5$	$1.14\ 10^5$	$1.19\ 10^5$	$1.21\ 10^5$	$1.22\ 10^5$	$1.24\ 10^5$	$1.29\ 10^5$
8 U (cm/sec)	107.17	114.07	129.20	135.25	138.94	146.61	163.50
9 $R_x = \frac{U.x}{\nu}$	$5.20\ 10^4$	$2.21\ 10^5$	$5.02\ 10^5$	$7.88\ 10^5$	$1.08\ 10^6$	$1.42\ 10^6$	$1.83\ 10^6$
10 α	1.0240	1.0127	1.0144	1.0407	1.0410	1.0158	1.0217
11 β	1.0110	1.0019	1.0029	1.0201	1.0201	1.0036	1.0105
12 Fr'	.723	.866	1.024	1.116	1.153	1.205	1.443
from measurement							
13 δ_d (cm)	.075	.129	.266	.247	.258	.216	.118
14 δ_d/x	.01505	.00645	.00665	.00414	.00323	.00213	.00104
15 x/k	5000	20000	40000	60000	80000	100000	115000
theor.							
16 δ_d/x	.0076	.0037	.0021	.0022	.0023	.0024	.0024
17 $\alpha \frac{\bar{U}^2}{2g}$ (cm)	5.23	6.65	8.33	9.37	9.79	10.62	13.12
18 H_p (cm)	25.22	24.27	24.09	24.42	24.52	24.76	25.72
19 C_D (Ippen)	.9924	.9896	.9732	.9751	.9740	.9785	.9879
20 Preston τ_o (N/m^2)	3.77	3.26	3.75	3.89	3.89	4.18	6.39
21 τ_o (N/m^2) velocity profile	1.99	1.97	2.23	4.22	4.27	4.25	3.43

3.3. Discussion of the results and conclusions

3.3.1. Boundary layer thickness on the crest

From the analysis of the experimental data (table III and IV), it can be seen that the boundary layer displacement thickness increases gradually at the upstream end of the horizontal crest (x = o), reaches its maximum value approximately at the middle of the crest (x = ½L) and decreases again towards the downstream end.

Two typical examples are shown in Fig. 18A and 18B. When studying these figures the different scales of waterdepth and displacement thickness should be kept in mind. In all cases, except for the case of the short weir-table (L = 40 cm) with the relatively low flow rate of Q = 25 ^{1}/sec, the observed boundary layer on the crest develops faster than on a plate in an infinite fluid. However, towards the downstream end of the weir the displacement thickness drops below the corresponding one in an infinite fluid. The experimentally resolved values of the relative boundary layer displacement thickness $\frac{\delta_d}{x}$ proved to be at most four times as high as the corresponding values of $\frac{\delta_d}{x}$ on a plate in an infinite fluid, with $R_t = 3.50^5$ and $k = 10^{-5}$ m, such as computed by Harrison {5}. This observation appears to be in contradiction to the previous statement of Delleur {2} and Nikuradse {17} i.e. that the boundary layer on the crest will develop more slowly than in an infinite fluid, because of the negative pressure gradient ($\frac{dD}{dx} < 0$) that occurs in the measuring section (acceleration of flow) of the weir. For this apparent contradiction some possible explanations can be found, when assuming that the numerical analysis of the adjusted velocity distribution profiles gives a realistic idea of the boundary layer displacement thickness on the crest.

1. In using the $\frac{\delta_d}{x}$ -curves from Fig. 5 an error in assessment of the relative roughness height $\frac{x}{k}$ causes an error in the resulting relative displacement thickness, on condition that the boundary layer is not laminar ($R_t > 3.10^5$). Since the roughness height of the weir table, k, is not precisely known and can only be accurately established from fully developed flow in open channels of pipes, the assumed value of 10^{-5} m is doubtful and therefore the comparative values of $\frac{\delta_d}{x}$ on flat plate are doubtful as well. Nevertheless, a relatively great increase of k (for instance 10^{-4} m) has not much influence on the resulting $\frac{\delta_d}{x}$ -value since the boundary layer is preponderantly laminar or just about to become turbulent ($R_x < R_t$) and consequently the error in assessment of k does not explain the discrepancy between theoretically predicted values of the

displacement thickness and experimental results. The question also arises from which point the distance x should be measured on the crest, in order to allow a justified comparison between experimental and theoretical values of $\frac{\delta_d}{x}$. Although some experiments by Hall {3} and Guersney {25} indicate that the boundary layer originates a short distance before the upstream end of the horizontal crest the error in assessment of the distance x is of minor importance and certainly does not explain the above mentioned discrepancy, because of the additional major effect of the flow curvature at the entrance of the structure.

2. The choice of the transition Reynolds number, too, is of some importance for the determination of the theoretical $\frac{\delta_d}{x}$-value. However, this R_t-value cannot be accurately estimated, but it is known that it is reduced by an increase in the roughness of the crest and side walls or the freestream turbulence, while it is increased by a favourable pressure gradient. Moreover, R_t-values higher than the here assumed value of $R_t = 3.10^5$ lead to even bigger differences between experimental and theoretical values of $\frac{\delta_d}{x}$, because the boundary layer remains laminar for a longer period of time. It may be concluded that the choice of $R_t = 3.10^5$ might be doubtful, but on the other hand does not explain the discrepancy mentioned above. The transition from laminar into turbulent boundary layer at $R_t = 3.10^5$ occurs for the short weir-table near the end of the crest (25 cm < x < 35 cm) and for the long weir-table already within halfway of the crest (20 cm < x < 40 cm).

3. From the two-dimensional velocity distribution across the weir in Fig. 21 it can be seen that the maximum velocity gradient on the crest occurs at approximately 5 cm from the side walls, which is in accordance with the measured shear stress distribution around crest and side walls (Fig. 22). It may therefore be concluded, that the boundary layer development on the center-line of the crest is influenced by the frictional resistence of the side walls. Of course this influence is absent in the case of a flat plate in an infinite fluid. The average displacement thickness over the wet cross-section will therefore be less than the displacement thickness measured on the center-line of the crest:

$$\frac{1}{W} \iint_A (1 - \frac{u}{U}) dA < \int_o^D (1 - \frac{u}{U}) dy$$

Possibly the frictional resistance of the side walls (rotational flow in a plane parallel to the crest) is a favourable condition for the boundary layer development on the center line of the crest, which is maximal there (see Fig. 21).

Consequently this effect should be taken into account when comparing boundary layer growth on the center line of the crest and growth on plates in infinite fluids.

4. Regarding the water surface profiles and pressure head levels on the weirs (Fig. 18A and B give examples) some useful observations can be made:

a. At the upstream end of the crest the surface profile curvature changes from convex upwards to concave downwards, and furthermore changes back again (drawdown curve) to convex upwards at the downstream end.

b. Changes in sign of curvature (points of inflection) occur at the positions for which the ratio H_o/x is approximately 0.8 and 0.2, the points of inflection coinciding with hydrostatic pressure distribution.

c. The pressure head upstream of the first point of inflection ($H_o/x < \sim 0.8$) is below the water surface and a strong positive pressure gradient exists here. Between the first and the second point of inflection ($\sim 0.8 < H_o/x$ 0.2) the pressure distribution is virtually hydrostatic, the converging practically straight streamlines are the cause of a negative pressure gradient ($\frac{dD}{dx} < 0$). At the downstream end ($H_o/x < \sim 0.2$) the drawdown of the water level causes a very strong negative pressure gradient, with pressure heads far below the water surface and the pressure head being zero for x = L. (See also Harrison {5}).

It may be concluded that at the upstream end of the crest, the boundary layer is enabled to develop faster than on a flat plate in an infinite fluid, because of the favourable positive pressure gradient, which depends largely on the ratios H_o/P and H_o/R. (Compare also equation 48 in section 2.2.5.) In the region where the surface profile is concave downwards, the boundary layer displacement thickness remains almost constant, while the influence of the negative pressure gradient on the development of δ, probably works against the favourable influence of the concave surface profile (with consequent slight positive pressure gradient, see also velocity profiles in Fig. 15). Unfortunately this cannot be proved, because no accurate pressure head recordings are available. The drawdown of the water surface and the consequent pressure gradient at the end of the weir, cause the boundary layer to decrease rapidly. The shape of the flow profile and the crest pressure heads are mainly responsible for the observed behaviour of the boundary layer on the crest and are probably the main reasons for the previously mentioned discrepancy between boundary layer developments on a weir crest and on a flat plate in an infinite fluid. For low heads ($H_o/P < 0.6$), the positive pressure gradient sharply decreases which explains the exceptional case for

L = 40 m and Q = 25 l/sec., where this discrepancy does not occur.

3.3.2. Shear stress distribution

The shear stress measured with the Preston tube over the center line of the crest, does not show a uniform increase with increasing velocity (see fig. 18), which is possibly due to the transition from laminar into turbulent boundary layer.

The comparitive values of τ_o (see table IV B and C) which are deduced from the velocity distribution within the boundary layer according to the Prandtl-von Karman velocity model for turbulent flow along smooth boundary, deviate strongly from the directly measured values. However, it must be taken into account that in fitting a regression line to the observation points within the boundary layer, the slope of the resulting line and hence the shear velocity

$$u_* = \left(\frac{\tau_o}{\rho}\right)^{\frac{1}{2}}$$

is very much influenced by inaccuracy of measurement. Moreover, Willis {16} has shown that the Prandtl-von Karman model can deviate rather much from velocities measured very close to the wall. Shear stress distribution measurements by Gosh and Roy {18} show the same discrepancy between the Preston-tube measurements of τ_o and those deduced from velocity distributions.

3.3.3. Comparative discharge coefficients

If one wishes to determine the discharge coefficient of a broad-crested weir from the analytically derived equation (Ippen):

$$C_D = \left(1 - \frac{\delta_d}{x} \cdot \frac{x}{B}\right)\left(1 - \frac{\delta_d}{x} \cdot \frac{x}{H_o}\right)^{3/2} \qquad \ldots\ldots\ldots (76)$$

the question immediately arises which distance should be used for the determination of the relative displacement thickness $\frac{\delta_d}{x}$ (Fig. 19).

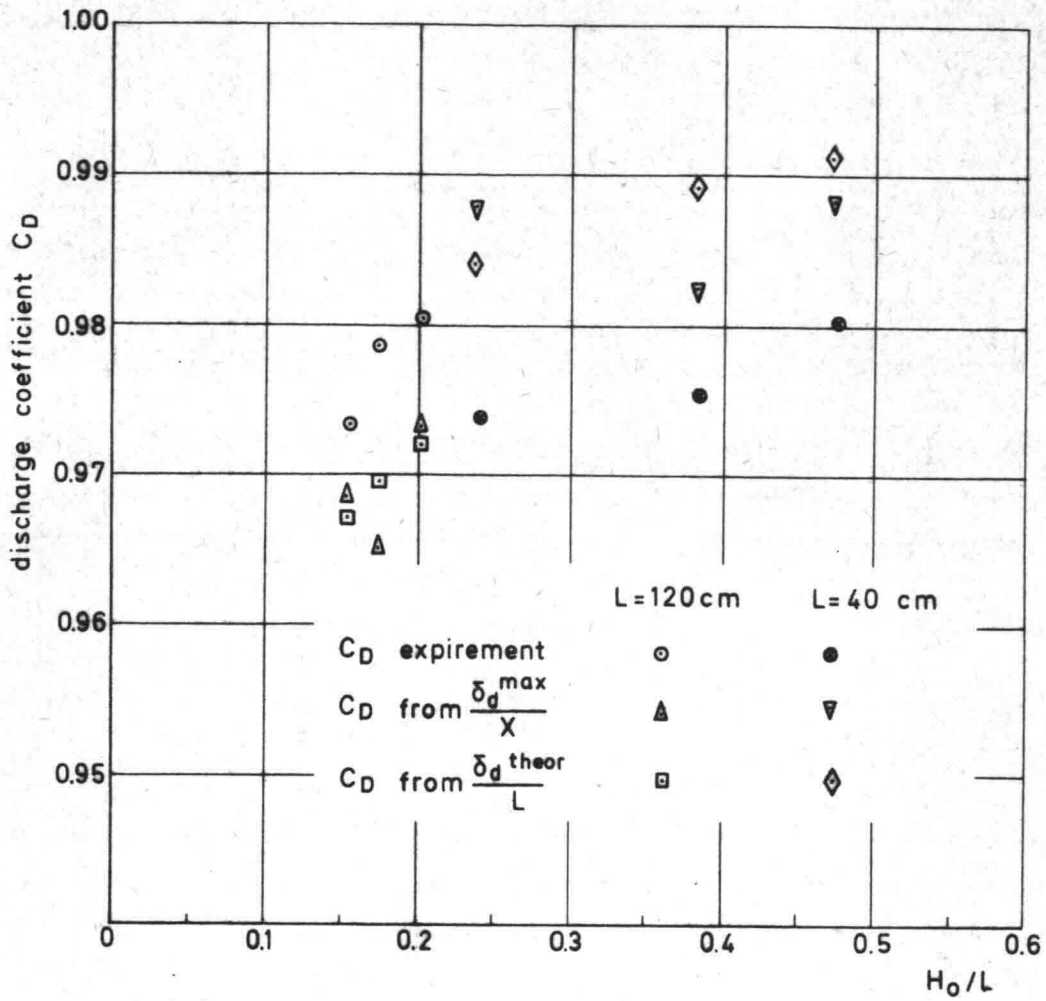

Fig. 19 Discharge coefficient data

According to the theory, the section where the flow becomes critical has to be reduced by the average displacement thickness multiplied by the wet perimeter (20). Hall {3} states, that δ_d reaches its maximum at a position where critical conditions occur and he assumes this to be not far from the upstream edge of the crest (because of separation of flow). Harrison {4} and Kalkwijk {6} assume, when using the results for boundary layers in infinite fluids, that critical conditions occur at the end of the measuring section, and therefore the length of the weir L should be inserted in the C_D-equation (76). (The error in assessment of the roughness height will have greater influence on the resulting value of δ_d!).

Adjusted Discharge Rate	Length of weir-table	$D_c = 2/3\ H_o$		$Fr' = 1$		$D_c = D_e/0.715$		location
Q_{ad} m^3/sec	L cm	D_c cm	x cm	D_c cm	x cm	D_c cm	x cm	of maximum δ_d cm
0.025	40	6.46	5-15	7.06- 6.08	5-15	6.25	5-15	5-15
0.050	40	10.24	15-20	10.30- 9.72	15-20	10.02	15-20	15-20
0.070	40	12.76	15-20	13.22-12.34	15-20	12.73	15-20	15-20
0.065	120	12.40	20	12.45-11.50	30-50	12.05	30-40	40-60
0.080	120	13.96	30-40	14.79-13.39	30-50	14.00	30-40	30-50
0.100	120	16.20	30-40	17.62-15.76	30-40	16.10	30-50	30-50

Table V: Location where critical depths occur (x = distance measured from upstream end of the horizontal crest).

In table V the locations are indicated where the critical state of flow should occur on the crest, when different principles are applied. The theoretical correction for boundary layer effects on the critical depth:

$$D_c = \frac{2}{3} H_o \pm \varepsilon \qquad \varepsilon \ll H_o$$

is very small, relative to the depth of flow and has therefore hardly any influence on the section where critical conditions occur. From the normal drawdown curve (33) in section 2.2.3. another criterion for the critical depth can be derived:

$$Fr' = \frac{\beta^{\frac{1}{2}} \cdot \bar{u}_c}{(g \cdot D_c)^{\frac{1}{2}}} = \beta^{\frac{1}{2}} \cdot Fr = 1$$

which is indicated in table III and IV on line 12 (see also Fig. 18). When the the empirically developed formula for the critical depth is applied on a free overfall structure {20}, a very good agreement with the two other criteria will be obtained:

$$\frac{D_e}{D_c} = 0.715$$

in which D_e = end - or brinkdepth.

The three criteria show a rather good agreement, if one realizes the limits of accuracy.

(Even $H_p = D + \alpha \frac{u^{-2}}{2g}$ reaches a minimum value in the same section, table III and IV, line 18). The first conclusion that can be drawn, is that the location of the position at which critical conditions occur, is within halfway of the crest, regardless of the different weir sizes. Furthermore, the crest section where the displacement thickness is maximal (also indicated in table V), virtually coincides with the critical section and in addition, δ_d does not change for $x/L > 0.3$.

The effect of the distance x, that corresponds with the used displacement thickness, on the computed C_D-value, is shown for two typical examples in Fig. 20. For the short weir table, the differences are of no importance and amount to a maximum of $\pm$ 0.5%, while on the long weir table the differences are much greater (maximum $\pm$ 2.0%). However, in the section where critical conditions occur ($0.3 < {}^{x}/_{L} \leq 0.6$) the C_D-values remain almost constant.

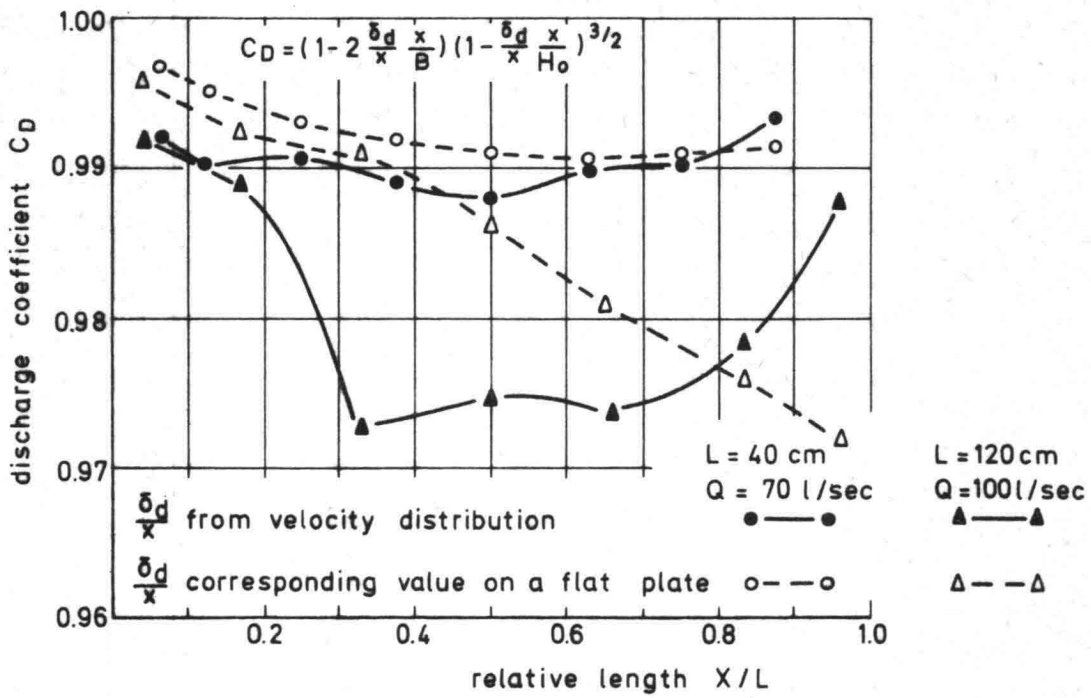

Fig. 20 Boundary layer development on the crest as related to C_D

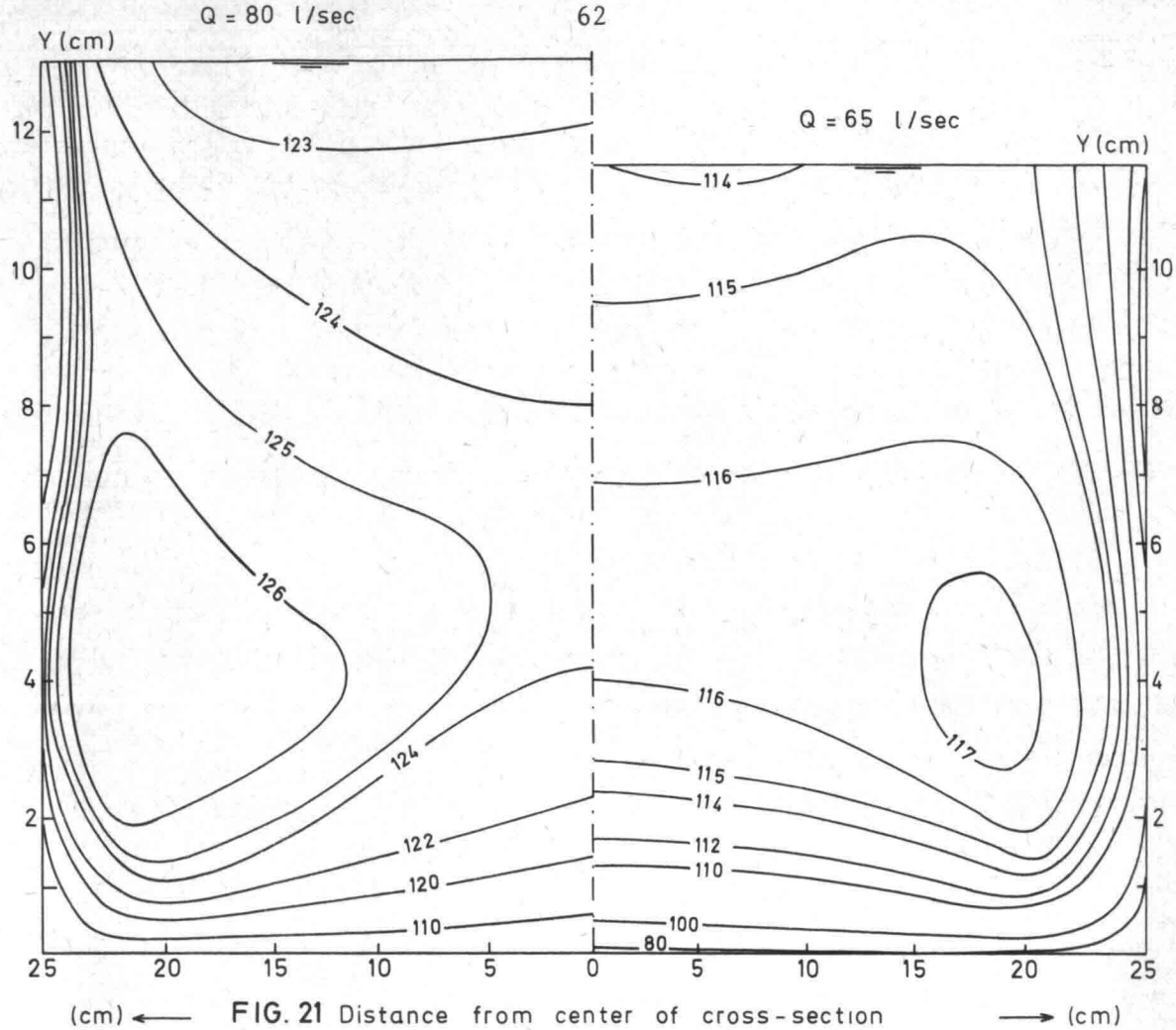

FIG. 21 Distance from center of cross-section

Velocity contour pattern in cross-section (X = 60 cm) L = 120 (cm)
(isovels in cm/sec)

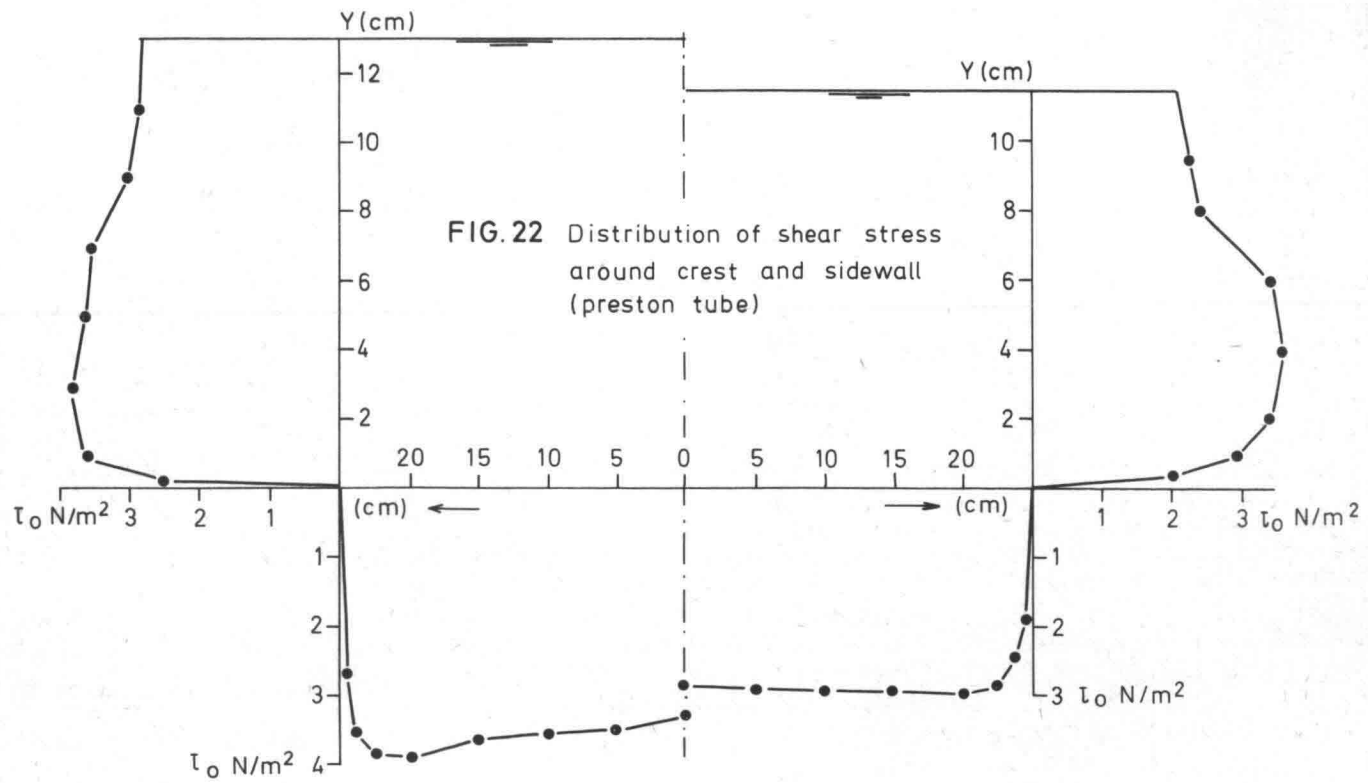

FIG. 22 Distribution of shear stress around crest and sidewall (preston tube)

Fig. 20 also shows the comparative C_D-values as derived from the theoretical boundary layer displacement thickness in infinite fluids by means of equation (76). It may be noticed that the greatest deviations of the resulting C_D-values from the earlier mentioned C_D-values (with δ_d deduced from velocity distribution) occur at the long weir-table, the maximum relative deviation being about 1.8% for $\frac{x}{L} = 0.33$, which lies just within the critical section.
In table VI several significant values of C_D, computed on the basis of different criteria for the relative displacement thickness, are compared with the experimental discharge coefficient C_D^{ex} data:

$$C_D^{ex} = \frac{Q_{ad}}{(\frac{2}{3})^{3/2} \cdot g^{\frac{1}{2}} \cdot B \cdot H_o^{3/2}}$$

Q_{ad} m^3/sec	h m	L m	p m	$\frac{u^2}{2g}$ m	H_o m	H_o/L	C_D^{ex}	$\frac{\delta_d}{x}^{max}$ 1)	C_D^m	$\frac{\delta_d}{L}^{th}$ 2)	C_D^{th}	H_o/P
0.025	.0957	0.40	0.25	.0011	.0968	.2420	.9739	.0123	.9881	.0023	.9844	.3872
0.050	.1503	-	-	.0032	.1535	.3875	.9755	.00853	.9825	.0022	.9894	.6140
0.070	.18063	-	-	.0052	.1915	.4788	.9801	.00511	.9880	.0021	.9913	.7660
.065	.1816	1.20	0.25	.0045	.1861	.1551	.9735	.00440	.9685	.0024	.9670	.7444
.080	.2033	-	-	.0062	.2095	.1746	.9788	.00390	.9652	.0024	.9695	.8380
.100	.2345	-	-	.0084	.2429	.2024	.9801	.00665	.9732	.0024	.9722	.9716

Table VI: Comparison between several discharge coefficients.

1. δ_d^{max}: maximum value of δ_d which has been measured
2. δ_d^{th} : theoretical value of δ_d, as computed for a flat plate in an infinite fluid, with x = L.

The accuracy of the experimental values C_D^{ex} can be estimated in the following way: adjusting the discharge (V-notch) in the laboratory model, an error in the reading of the water level in a stilling well is made, with an average of $\pm$ 0.03 cm on an average head of 30 cm, which yields a relative error of 0.1%. Assuming that the same error can be made in reading the head H_o (stilling well) in the approach flume, then the total relative error in C_D^{ex} amounts to:

$$R.E = (0.1)^{3/2} + (0.1)^{3/2} = 0.06\,\%$$

If furthermore, an error of 0.5% in the rating curve of the V-notch is present, then the final relative error in C_D^{ex} will, in the most unfavourable case, be 0.56%.

From table VI and Fig. 19, it may be concluded, that the agreement between values of C_D^{ex} and C_D^{m} (on basis of δ_d^{max}/x) for the long weir-table ($L = 120$ cm, $H_o/L < 0.20$) is good, with a maximum relative deviation of 0.7%, which is in the same order as the measurement error in C_D^{ex}. Despite the doubtful assumption of using theoretical boundary layer growth in infinite fluids for the analytical determination of the discharge coefficient (on the basis of δ_d^{th}/L), the differences between the values of C_D^{th} and C_D^{m} are of minor importance. Since $C_D^{ex} > C_D^{m}$ the values of δ_d^{max} are obviously too high, which might be due to the fact that δ_d in the centre line is not representative (too high) for the whole crest.

On the other hand it must be taken into account, that the C_D-equation was obtained by assuming that δ_d is independent of the depth of flow D, which is only true for high Reynolds numbers and for rough boundaries. This does not apply to the here used scale models. With experiments on the short weir-table ($L = 40$ cm), the divergence between C_D^{ex} and C_D^{m} or C_D^{th} is stronger, and amounts to a maximum of 1.5 %.

Two possible reasons can be indicated:

1. The velocity measurements on the short weir table were less accurate and the introduced errors could not be easily reproduced.
2. The limit of validity of the C_D-equation (76) might be exceeded for H_o/L ranging between 0.24 and 0.50 on the short weir-table, since the theory of analytical discharge coefficients assumes straight and parallel flow on the crest.

The fact that $C_D^{m} > C_D^{ex}$ indicates however, that the observed δ_d^{max} is too small. This might be due to too low velocity measurements caused by improper setting of the "wall-Pitot" tube. Here again the differences between C_D^{m} and C_D^{th} are of relatively minor importance.

Unfortunately the number of available discharge coefficient data is too small to be of absolute statistical significance, and no reliable band width of scatter or accuracy of agreement with theory can be found.

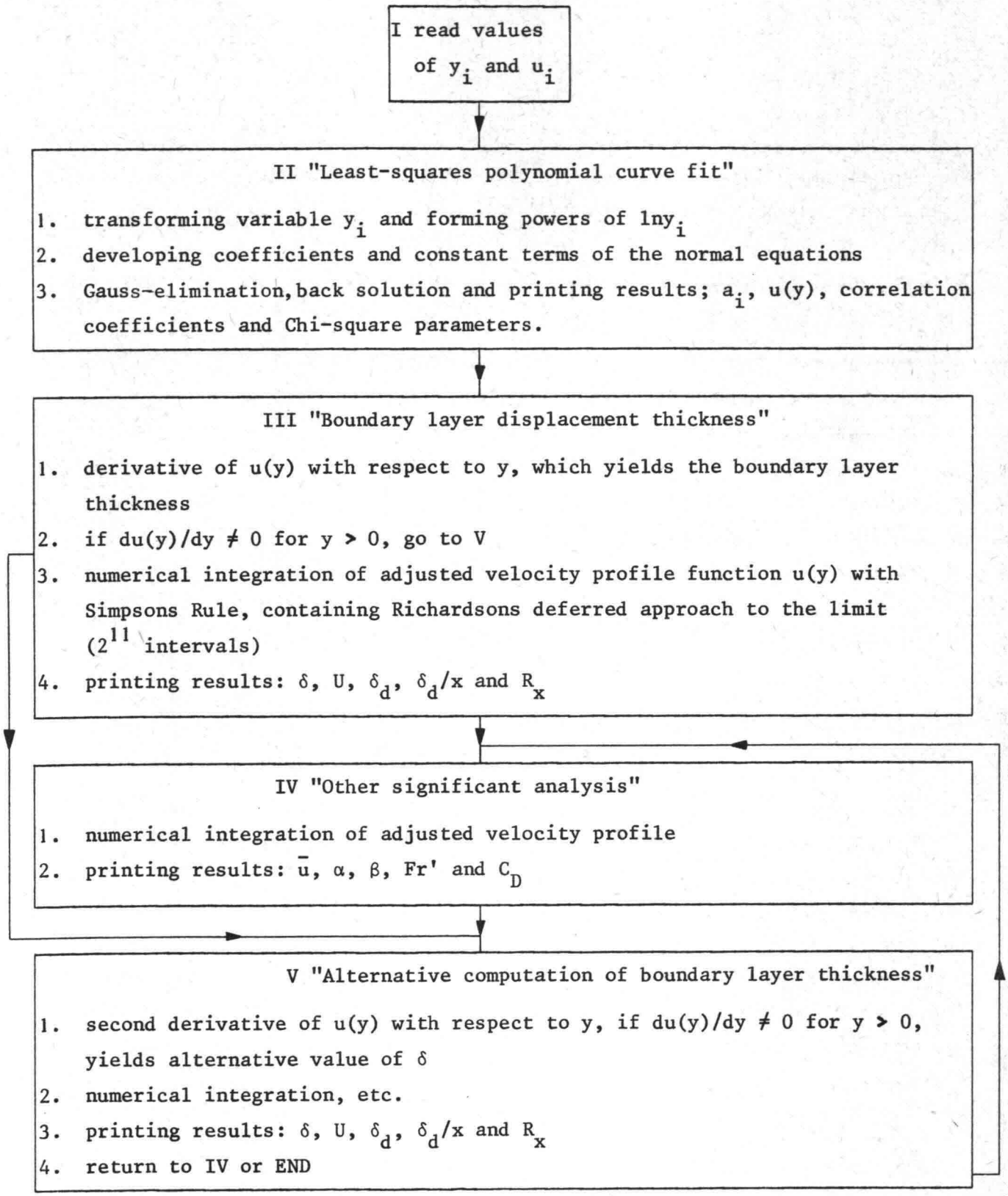

Fig. 23 Schematic description of FORTRAN IV program (CDC-3200) for data processing.

3.3.4. Conclusions

1. The measuring equipment used (Pitot-tubes and electronical recording) allow a realistic view of the shape of the velocity distributions on the rectangular broad- crested weir, with a long horizontal crest. More accurate calibration of the "wall-Pitot" tube should improve the results of measurement.

2. The applied regression model for the velocity distribution function (third degree polynominal function with respect to the natural logarithm of the independent variable y) allows a satisfactory adjustment of the velocity measurements as well as the possibility to determine efficiently a number of characteristic shape factors of the velocity profile.

3. The boundary layer displacement thickness on the crest of the weir for $x/L < 0.8$ proved to be higher than the corresponding values of δ_d resulting from boundary layer theory on a flat plate in an infinite fluid, despite the theoretical considerations of Delleur {2} and Kalkwijk {6}, that the boundary layer on the crest would develop more slowly because of the unfavourable negative pressure gradient. The main reasons for this must be sought in conclusions 4 and 5.

4. From a theoretical point of view it is not allowed to consider the boundary layer development on the crest of the weir as similar to the development of a boundary layer on a flat plate in an infinite fluid, since pressure and flow conditions are not comparable.
The favourable positive pressure gradient at the entrance of the weir and probably the concave downwards flow profile as well (with a consequent positive pressure gradient) cause the boundary layer at the upstream half of the crest to develope more rapidly than it does on a flat plate, whilst the negative pressure gradient at the downstream end of the crest ($x/L > 0.2$) reduces the boundary layer to a point where the corresponding displacement thickness drops even below the corresponding one of a flat plate in an infinite fluid. However, only more accurate measurements of the actual longitudinal pressure distribution on the crest can prove whether these assumptions about the pressure gradient are reasonable.

5. The boundary layer displacement thickness on the crest, which is measured on the center line of a cross section, is higher than the average displacement thickness along the wet perimeter of the cross section. Inserting the one dimensional displacement thickness on the centerline in the Ippen-equation therefore results in too low values of C_D.

6. The location of the position at which critical conditions occur, is not at the end, but within halfway of the measuring section. As a matter of fact, the assumption that critical conditions occur at the end of the crest, is based on straight and parallel flow over the weir.

7. The agreement between discharge coefficients computed on the basis of the Ippen-equation (inserting measured values of the boundary layer displacement thickness) and experimental coefficient data of the long weir-table ($H_o/L < 0.20$) was found to be satisfactory. The exact distance from the upstream end of the crest where the measured displacement thickness was obtained from, has (within a certain range, $0.3 < \frac{x}{L} < 0.7$) not much influence on the computed C_D-value. The validity of the Ippen-equation for the experimental data of the short weir-table ($H_o/L > 0.24$) is doubtful. However the number of available data is insufficient and has to be increased in order to yield more reliable information. Moreover, the limit at which the critical depth theory ceases to hold, does not only depend on the ratio H_o/L, but also on the second significant parameter describing the flow over the weirs, i.e. the ratio H_o/P.

8. If the results for boundary layers in infinite fluids (non-accelerating flow) are used in order to compute the discharge coefficients (with $x = L$) for weirs with low relative heads ($H_o/L < 0.25$), the agreement with experimental coefficient data is satisfactory (relative deviation less than 1%). Without using laboratoy scale models, this method allows an appropriate prediction of the actual discharge of field installations, if one is not interested in a one percent accuracy.

9. From the experiments on the long weir-table it can be seen, that the difference between theoretical discharge (frictionless case of non-viscous fluid) and actual discharge amounts to a maximum of 2.6% ($C_D^{ex} = 0.974$), which is assumed to be the result of viscous effects. The C_D^{th}-value in that case (in which the results of boundary layers in infinite fluids are used -Harrison-), amount up to 0.967 (3.3% less than unity). This means that the reduction in discharge as a consequence of the boundary layer effects, can be estimated by the proposed method of Harrison {4} and Kalkwijk {6} with a relative error of approximately 25%. For the experiments on the short weir-table this error is even more than 50%. It must however be borne in mind, that during the experiments a complex combination of instrumental, methodological, personal and sampling errors are introduced, which are difficult or even impossible to reproduce.

LIST OF SYMBOLS

The following symbols were adopted for use in this Paper:

A : area of wet cross section

a_i : parameter of regression model for velocity distribution

B : width at water level or width of a rectangular cross section

C_{av} : average correction factor of the "Wall-Pitot" tube

C_v : correction coefficient in discharge relationship to measured head over the weir

C_D : Standard discharge coefficient

C_f : total dimensionless friction factor (or drag coefficient)

c_f : local dimensionless friction factor

c : suffix referring to critical state

D : depth of flow on crest

D_e : end depth or brink depth

d : external diameter of dynamic tube of Preston

F : total shear over a certain distance

Fr or Fr': Froude number

f : function

g : acceleration due to gravity

H : shape factor of boundary layer

H_o : specific energy head above the crest

H_{o_1} : total energy head in the approach channel

H_p : energy head outside the boundary layer

h : measured head upstream of weir crest

h_o : depth of flow over the weir at the upstream edge of the crest

k : equivalent roughness height of Nikuradse

L : lenght of horizontal crest. L also denotes dimension of length in prototype structure

l : denotes dimension of length in model

ln : natural logarithm

log : decimal logarithm

M : constant, which is a measure for the curvature of flow at the upstream end of the crest

m : suffix for model

N : ratio of length of scale model in relation to prototype

n : coordinate in the direction normal to the flow in the Euler-equations

P : crest-height (above the bottom or the approach channel)

P_g : Gaussian standard normal depth variable

p : local pressure

pr : suffix for prototype

Q : discharge rate

Q^{th} : theoretical discharge rate

Q_{ad} : adjusted discharge rate in laboratory

R : radius of rounded off nose at entrance of weir

R_e : Reynolds number based on hydraulic radius R_h

R_{H_o} : Reynolds number based on specific head H_o

R_h : hydraulic radius

R_x^* : length Reynolds number

R_t : transition Reynolds number

r : radius of curvature of streamlines

S : sum of squares of departures

S_o : bottom slope

S_e : energy slope

U : free-stream velocity outside the boundary layer or velocity at outer edge of the boundary-layer.

u : point velocity in x direction at distance y from boundary

u_t : instantaneous velocity at time t in turbulent flow

u_m : velocity at which $y = y_m$

$\bar{u}$: average velocity in a cross section

u_* : shear velocity

T : time dimension in prototype

t : elapsed time or time dimension in model

W : wet perimeter

x : coordinate in the direction of flow, measured along the boundary

x_t : distance from upstream edge of the crest or flat plate to the point where the transition from laminar into turbulent boundary layer starts

y : vertical distance above the weir crest

y_m : vertical distance above the weir crest where $u = u_m$

α : energy velocity distribution coefficient

β : momentum velocity distribution coefficient

γ : weight factor for transition boundary layer

δ : boundary layer thickness

δ_d : boundary layer displacement thickness

δ_m : momentum thickness of the boundary layer

δ_e : energy thickness of the boundary layer

ε : coefficient

κ : von Karmans turbulence coefficient

μ : dynamic viscosity

ν : kinematic viscosity

ρ : density of fluid

τ_o : shear stress at the flow boundary

ϕ : top angle of V-shaped broad-crested weir

ψ : function

1 : suffix for approximated critical section

REFERENCES

1. Ippen, A.T., Channel transitions and controls. Engineering Hydraulics. John Wiley and Sons, New York, 1950, 525-528.

2. Delleur, J.W., The boundary layer development on a broad-crested weir. Proceedings of the fourth Midwestern Conference on fluid mechanics. Purdue University, 1955, 183-193.

3. Hall, G.W., Analytical determination of the discharge characteristics of broad-crested weirs using boundary layer theory. Proc. Instn. Civ. Engrs., 1962, 22, 172-190.

4. Harrison, A.J.M., The streamlined broad-crested weir. Proc. Civ. Engrs., 1967, 38 (Dec.) 657-678.

5. Harrison, A.J.M., Boundary layer displacement thickness on flat plates. Proc. Am. Soc. Civ. Engrs., 1967, 93 HY4 (July) 79-91.

6. Kalkwijk, J.P.Th., A note on the discharge of critical depth measuring devices with arbitrary shape. Proc. Instn. Civ. Engrs., 1970, 47 (Oct.) 227-238.

7. Smit, M., De invloed van de grenslaag op de afvoer van een horizontale, vlakke meetoverlaat. Lab. Hydraulica en Afvoerhydrologie, Landbouwhogeschool Wageningen, 1970.

8. Pitlo, R.H., Stroomsnelheids- en schuifspanningsmetingen langs gladde en ruwe wanden. Nota no. 16, Lab. Hydraulica en Afvoerhydrologie, Landbouwhogeschool Wageningen, 1970.

9. Gaasbeek, G.H., Een meetopstelling voor het dynamisch meten van enige hydraulische grootheden. Nota no. 23, Lab. Hydraulica en Afvoerhydrologie, Landbouwhogeschool Wageningen, 1971.

10. British Standard 3680: Methods of measurement of liquid flow in open channels. Part 4B: 1969.

11. Schlichting, H., Boundary layer theory. 4th ed., McGraw' Hill Book Co. Inc. New York, 1962.

12. Granville, P.S., The frictional resistance and turbulent boundary layer of rough surfaces. Report No. 1024, David Taylor Model Basin, Washington, D.C. June, 1958.

13. Dhawan, S. and Narasimha R., Some properties of boundary layer flow during transition from laminar to turbulent motion. Journal of Fluid Mechanics, Vol. 3, Jan., 1958, pp. 418-436.

14. Kalkwijk, J.P.Th., A note on the discharge of critical depth measuring devices with arbitrary shape. DISCUSSION. Proc. Instn. Civ. Engrs., 1971, 49 (Aug.) 503-510.

15. Yen, B.C. and Wenzel H.G., Jr., Dynamic equations for steady spatially varied flow. Proc. Am. Soc. Civ. Engrs., 1970, 96 (Mar.) HY3, 801-814.

16. Willis, J.C., A new mathematical model for the velocity distribution in turbulent shear flow. Journal of Hydraulic Research 10 (1972) No. 2.

17. Nikuradse, J., Untersuchungen ueber die Stroemung des Wassers in konvergenten und divergenten Kanaelen. Forschungsarb. Verein. Deut. Ingr. No. 289, 1929.

18. Gosh, S.N. and Roy, N., Boundary shear distribution in open channel flow. Proc. Am. Soc. Civ. Engrs., 1970, 96 (April) HY4, 967-995.

19. Krayenhoff van de Leur, D.A., Hydraulica, Collegedictaat, 1972, Landbouwhogeschool Wageningen, Afd. Hydraulica en Afvoerhydrologie.

20. Rouse, H., Discharge Characteristics of The Free Overfall. Civil Engineering, April 1936.

21. Rouse, H. et. al., Advanced Mechanics of Fluids. John Wiley and Sons Inc. New York, 1959.

22. Jaeger, C., Engineering Fluid Mechanics, Blackie and Sons, Ltd., London England, 1956.

23. Chow, V.T., Open Channel Hydraulics. McGraw' Hill Book Company, Inc. New York, 1959.

24. Lakshmana Rao, Nagar, S. and Jagannadha Rao M.V., Characteristics of Hydrofoil Weirs. Proc. Am. Soc. Civ. Engrs., 1973, HY2, 259-283.

25. Guernsey, R., The Boundary Layer in a Broad-crested weir. Civil Engrs., Thesis, Columbia University, New York, May 1940.